Climate Dynamics (2021) 56:701–725
https://doi.org/10.1007/s00382-020-05501-1

The dominant North Pacific atmospheric circulation patterns and their relations to Pacific SSTs: historical simulations and future projections in the IPCC AR6 models

Shangfeng Chen[1] · **Bin Yu**[2] · **Renguang Wu**[3] · **Wen Chen**[1] · **Linye Song**[4]

Received: 1 May 2020 / Accepted: 9 October 2020 / Published online: 18 October 2020

Abstract
The first two leading modes of the North Pacific atmospheric variability, the Aleutian Low (AL) and North Pacific Oscillation (NPO), in boreal winter and their relations to the North American and Eurasian surface temperature, El Niño–Southern Oscillation (ENSO), Pacific Decadal Oscillation (PDO), and Victoria Mode (VM) are explored in 20 coupled climate models which participated in the sixth Assessment Report of the Intergovernmental Panel on Climate Change. The historical simulations of these models can well reproduce spatial structures and amplitudes of the winter AL and NPO, as well as their associations with North American and Eurasian surface air temperatures. The close connections of the winter AL with ENSO and PDO, as well as the linkage between the NPO and VM could also be well simulated. However, most of the models lack the capability in simulating the impact of the winter ENSO on the NPO. This deficiency is mainly attributed to westward shifts of the ENSO-related sea surface temperature and precipitation anomalies in the tropics and ENSO-induced atmospheric teleconnections over the North Pacific in the models. Spread in the ENSO's amplitude also contributes partly to the diversity of the ENSO–NPO relation among the models. Under the SSP2-RCP4.5 forced climate change projection, projected changes in the amplitudes and centers of the AL and NPO exhibit large uncertainties across the 20 models. The close connections of the AL with ENSO and PDO, and the NPO with VM are still robust in the warming climate. Most models project an increase (a decrease) in the AL–PDO (NPO–VM) relationship. However, there exists a large uncertainty in the projected changes of the AL–ENSO relationship, which is partly attributed to the large divergence in the projected changes of the ENSO's amplitude among the models.

Keywords IPCC-AR6 · Aleutian Low · NPO · ENSO · PDO · Victoria mode · Historical simulation · Climate change projection

1 Introduction

North Pacific atmospheric variations and their close connections with the underlying sea surface temperature (SST) variability provide important sources of predictability for subseasonal-interannual climate predictions over many parts of the world, especially over Eurasia and North America (Namias 1969, 1972; Davis 1976; Vimont et al. 2001, 2003; Yoon and Yeh 2010; Yeh et al. 2011; Yu and Kim 2011; Chen et al. 2013a, b; Kim et al. 2014; Song and Duan 2015; Yeh et al. 2015). Hence, it is of great importance to improve our understanding of the North Pacific atmospheric variability as well as its linkages to the Pacific SST.

The first Empirical Orthogonal Function (EOF) mode of the interannual atmospheric anomalies in the North Pacific generally represents the Aleutian Low (AL) variation or

✉ Shangfeng Chen
chenshangfeng@mail.iap.ac.cn

[1] Center for Monsoon System Research, Institute of Atmospheric Physics, Chinese Academy of Sciences, Beijing, China

[2] Climate Research Division, Environment and Climate Change Canada, Toronto, ON, Canada

[3] School of Earth Sciences, Zhejiang University, Hangzhou, China

[4] Institute of Urban Meteorology, China Meteorological Administration, Beijing, China

the Pacific North American teleconnection pattern (PNA) (Wallace and Gutzler 1981; Yu et al. 2007; Yu and Kim 2011; Song and Duan 2015; Yu and Lin 2019; Chen et al. 2020). AL could be regarded as a surface manifestation of the PNA (Wallace and Gutzler 1981; Terada and Hanzawa 1984; Alexander et al. 2002; Chen et al. 2020). An enhanced (a weakened) AL is featured by negative (positive) SLP anomalies and an anomalous cyclone (anticyclone) around the Aleutian Islands (Yu and Kim 2011; Song and Duan 2015; Chen et al. 2020). AL is one of the most important components of the East Asian winter monsoon (EAWM) system (Chen et al. 2000; Zhou et al. 2007). It has close relations with the Arctic Oscillation (Thompson and Wallace 1998, 2000), the El Niño–Southern Oscillation (ENSO; Wang et al. 2000; Alexander et al. 2002), and the Pacific Decadal Oscillation (PDO; Latif and Barnett 1996; Mantua et al. 1997; Pierce et al. 2001). ENSO exerts impacts on the AL variation via triggering a PNA-like atmospheric teleconnection originated from the tropical Pacific convection anomaly (Gershunov and Barnett 1998; Alexander et al. 2002; Yu and Kim 2011; Leung et al. 2017). On the other hand, the formation of the PDO, the leading mode of North Pacific decadal SST anomalies, is found to be attributed mainly to the AL-related atmospheric forcing (Latif and Barnett 1996; Mantua et al. 1997; Pierce et al. 2001). Hence, AL plays a crucial role in connecting the ENSO and PDO and in relaying impacts of the tropical SST on extratropical climate anomalies. In addition, the AL variation influences the interaction between the low frequency mean flow and synoptic-scale eddies over the North Pacific (Lau 1988; Chen et al. 2020).

The second EOF mode of the atmospheric variability over the North Pacific represents the North Pacific Oscillation (NPO) (Linkin and Nigam 2008; Yu and Kim 2011; Chen and Song 2018; Chen et al. 2020). NPO is characterized by a meridional dipole structure of SLP anomalies between the subtropical and mid-latitude North Pacific (Wallace and Gutzler 1981; Linkin and Nigam 2008; Yu and Kim 2011). Linkin and Nigam (2008) demonstrated that NPO is the surface manifestation of the western Pacific (WP) pattern. The WP pattern is generally defined as the second EOF mode of 500-hPa geopotential height anomalies over the North Pacific (Linkin and Nigam 2008). NPO is an important atmospheric intrinsic mode, whose formation and maintenance are due largely to the interaction between the low-frequency mean flow and synoptic-scale eddies (Rogers, 1981; Lau 1988; Wettstein and Wallace 2010; Linkin and Nigam 2008). The positive phase of the NPO, featured by positive SLP anomalies over the northern subtropics, is associated with a northward movement of the Asian-Pacific Jet and a downstream intensification of the North Pacific storm track activity (Lau 1988; Wettstein and Wallace 2010). Besides the eddy-related process, studies indicated that the tropical ENSO-related SST anomalies could also influence the NPO via atmospheric teleconnections (Di Lorenzo et al. 2010; Furtado et al. 2012; Pak et al. 2014).

Both the AL and NPO variations exert substantial impacts on weather and climate over many regions of the globe. The AL could impact the formations of pack ice around the Bering sea (Overland and Pease 1982; Rodionov et al. 2005), surface air temperature and precipitation over North America (Ge and Gong 2009; Harding and Snyder 2015), precipitation over south China (Song and Duan 2015), tropical cyclone activities over tropical western Pacific (Choi and Cha 2017), and the EAWM (Chen et al. 2000) and Australian summer monsoon (Zhu and Wang 2010). A recent study indicated that the variation in the AL intensity in March has a significant influence on the following winter ENSO outbreak (Chen et al. 2020). Regarding the NPO, studies indicated that it could also exert impacts on the surface air temperature and precipitation over Eurasia and North America (Linkin and Nigam 2008; Chen and Song 2018). In addition, NPO is found to be a dominant forcing in the formation of the Victoria Mode (VM) (Bond et al. 2003; Ding et al. 2015) and the North Pacific Gyre Oscillation (NPGO) (Di Lorenzo et al. 2008; Chhak et al. 2009). VM is the second EOF mode of SST anomalies in the extratropical North Pacific, and the NPGO represents the second EOF mode of sea surface height in the central and eastern North Pacific. Furthermore, studies have demonstrated that the winter NPO is an important trigger for the outbreak of ENSO events in the following winter via the seasonal footprinting mechanism (Vimont et al. 2001, 2003; Park et al. 2013).

Given the pronounced impacts of the AL and NPO on the global climate and their close relationships with the air–sea interaction over the North Pacific, characterizing and understanding these two dominant atmospheric modes over the North Pacific in the state-of-the-art climate models is of great importance for studies of climate variability, change and predictability. Several studies have evaluated performances of the climate models that participated in Phases 3 and 5 of the Coupled Model Intercomparison Project (CMIP) in capturing the AL and NPO (Furtado et al. 2011; Gan et al. 2017; Chen et al. 2018; Wang et al. 2019). Based on CMIP3 simulations, Furtado et al. (2011) found that CMIP3 has a relatively good ability in capturing the AL–PDO relationship, whereas most models lack the capability in simulating the second atmosphere–ocean coupled mode over the North Pacific, which represents the connection of the NPO and VM or NPGO. Chen et al. (2018) found that most CMIP5 models could reasonably well reproduce the spatial structures of the winter PNA and NPO. However, the amplitudes of the simulated PNA and NPO in most models are much stronger compared to the observed.

A new suite of climate model simulations has been produced in CMIP6 for the latest sixth Assessment Report

(AR6) of Intergovernmental Panel on Climate Change (IPCC). One aim of the present study is to evaluate the performance of these latest climate models in simulating the AL and NPO and their relationships to the ENSO, PDO and VM. Furthermore, we analyze climate change projections of the winter AL and NPO in terms of their spatial distribution and amplitudes as well as the projected changes in their connections with the ENSO, PDO, and VM in a warming climate. The remainder of this paper is organized as follows. Section 2 describes the methods and data employed in the present study. Section 3 evaluates the performance of 20 CMIP6 models in capturing the observed wintertime AL and NPO patterns, and their associations with the Pacific SST and Eurasian and North American SAT anomalies. Section 4 examines projected changes in the spatial patterns and amplitudes of the winter AL and NPO, as well as responses of the AL–ENSO/PDO and NPO–ENSO/VM connections with global warming. Section 5 provides a summary and discussion.

2 Data and methodology

2.1 Observational and reanalysis data

The monthly mean SLP data is obtained from the National Centers for Environmental Prediction–National Center for Atmospheric Research reanalysis (NCEP–NCAR; Kalnay et al., 1996), which has a horizontal resolution of 2.5°×2.5° and is available from January 1948 to the present. The monthly mean SST data is derived from the National Oceanic and Atmospheric Administration (NOAA) Extended Reconstructed SST version 5 (ERSSTv5) dataset (Huang et al. 2017). The ERSSRv5 SST dataset is available from January 1854 to the present and has a horizontal resolution of 2.0°×2.0°. The monthly mean surface air temperature (SAT) is extracted from the University of Delaware Air Temperature & Precipitation version v5.01, which is available from January 1900 to December 2017 and on a 0.5°×0.5° latitude–longitude grid (Matsuura and Willmott 2009). In the following analysis, the SLP from the NCEP–NCAR reanalysis, SST from the ERSSTv5 and SAT from the University of Delaware are considered as "observational" data for the convenience of description.

2.2 CMIP6 model outputs

This study employs the outputs from 20 global coupled models currently available in CMIP6. Detailed descriptions of the CMIP6 models used in this analysis are listed in Table 1, including the model names, modelling centers and horizontal resolutions. We employ two sets of simulations from these coupled climate models outputs, including (1) the historical simulations, which are forced by the observed anthropogenic and natural forcings for the period of 1850–2014, and (2) the climate change

Table 1 Descriptions of the CMIP6 models employed in this study

Model Name	Modeling centers	Horizontal resolution (latitude × longitude)
ACCESS-CM2	CSIRO-ARCCSS, Australia	144 × 192
ACCESS-ESM1-5	CSIRO, Australia	145 × 192
BCC-CSM2-MR	Beijing Climate Center, China	160 × 320
CAMS-CSM1-0	Chinese Academy of Meteorological Sciences, China	160 × 320
CanESM5	CCCma, Canada	64 × 128
CESM2	NCAR, USA	192 × 288
CESM2-WACCM	NCAR, USA	192 × 288
CNRM-CM6-1	CNRM-CERFACS, France	128 × 256
CNRM-ESM2-1	CNRM-CERFACS, France	128 × 256
FGOALS-f3-L	IAP-CAS, China	180 × 288
FGOALS-g3	IAP-CAS, China	80 × 180
GFDL-ESM4	NOAA-GFDL, USA	180 × 288
HadGEM3-GC31-LL	Met Office Hadley Centre, UK	144 × 192
IPSL-CM6A-LR	IPSL, France	143 × 144
MIROC6	JAMSTEC, AORI, NIES, and and R-CCS, Japan	128 × 256
MIROC-ES2L	JAMSTEC, AORI, and R-CCS, Japan	64 × 128
MPI-ESM1-2-HR	Max Planck Institute for Meteorology, Germany	192 × 384
MRI-ESM2-0	Meteorological Research Institute, Japan	160 × 320
NorESM2-LM	CICERO, NERSC, NILU, UiB, UiO, and UNI, Norway	96 × 144
UKESM1-0-LL	Met Office Hadley Centre, UK	144 × 192

projection simulations over 2015–2100, which are forced by the update of RCP4.5 scenario based on SSP2 (denoted as SSP2-RCP4.5) (Eyring et al. 2016). SSP2-RCP4.5 has a similar range of forcings as those in the RCP4.5, but fills several forcing gaps by considering the role of specific forcings such as land use and short-lived species and the effect of a peak and decline in the forcings (Eyring et al. 2016). As a number of models just provide one member run in the historical or the future projection simulations, this analysis only uses the first run ("r1i1p1") of each model for a fair comparison.

We focus on boreal winter (NDJFM-average) during which both the AL and NPO are most prominent (Yu and Kim 2011; Song and Duan 2015; Chen et al. 2020). Model outputs over the periods of 1948/49–2013/14 and 2033/34–2098/99 (both containing 66 winters) represent the past and future climates, respectively. The projected change is defined as the difference between 2033/34–2098/99 and 1948/49–2013/14. Long-term trends of all variables considered in each period have been removed in analyzing the internal variability. Significance levels of regression and correlation coefficients in the observation and a given model are estimated based on the two tailed student's *t* test. The multi-model ensemble mean (MME) is calculated as the average of all individual models. Specifically, we first calculate anomalies in each model, and then average those to obtain the ensemble mean. Furthermore, following previous studies (Deser et al. 2012; Kucharski and Joshi 2017; Joshi and Ha 2019), the MME anomaly derived from a linear regression is considered to be significant at the 95% confidence level when it meets the following criterion:

$$|MME\_var| \geq \frac{std_{var} \times \lambda}{\sqrt{N}},$$

where $|MME\_var|$ represents the absolute value of the MME anomaly, *std_var* denotes the standard deviation of the anomalies among the multi-models, N is the number of models considered, and λ is equal to 1.96.

In this study, the AL and NPO indices in the observation are calculated in the following three steps. First, an EOF analysis is performed to the observed and linearly detrended winter SLP anomalies over the extratropical North Pacific region (20°–70° N, 120° E–100° W) for the period of 1948/49–2013/14. Second, the first and second EOF modes are employed to represent the AL and NPO patterns, respectively, as generally used in previous studies. Third, the observed AL (NPO) index is obtained by projecting the observed and de-trended winter SLP anomalies onto the first (second) EOF mode. Slight changes of the North Pacific region used in the EOF analysis lead to very similar results (not shown). The AL (NPO) indices in the CMIP6 model simulations are obtained by projecting the simulated and linearly de-trended winter SLP anomalies onto the observed first (second) EOF mode.

We use similar methods to define the PDO and VM indices in the observation and CMIP6 model simulations. Specifically, the first and second EOF modes of the observed and linearly de-trended SST anomalies over the North Pacific region (20°–65° N, 120° E–100° W) are used to represent the PDO and VM patterns, respectively. The PDO (VM) indices in the observation and CMIP6 model simulations are then obtained by projecting the corresponding de-trended SST anomalies onto the PDO (VM) spatial pattern.

Following Taylor (2001) and Chen et al. (2013a, b), we estimate performances of the models in simulating spatial patterns of winter AL, NPO, PDO and VM based on the following equation:

$$Skill = \frac{(1+r)^2}{\left(RSD + \frac{1}{RSD}\right)^2}$$

where r denotes spatial correlation between the observed and simulated anomalies. *RSD* indicates the ratio of pattern standard deviation of model simulation against that in the observed.

3 AL and NPO in historical simulations

In this section, based on the observation and historical simulations over 1948/49–2013/14, we first evaluate the capability of the CMIP6 models in simulating the wintertime AL and PDO patterns and the associations of the winter AL with the Eurasian and North American SAT, ENSO and PDO. We then examine the models' ability in characterizing the NPO pattern and the relations of NPO to SAT and SST. Finally, we discuss the factors responsible for biases of the NPO–ENSO connections among the models.

3.1 AL

Figure 1a displays the spatial distribution of simultaneous SLP and 850-hPa wind anomalies regressed upon the normalized winter AL index during 1948/49–2013/14 based on the observational data. For a positive AL phase, pronounced negative SLP and cyclonic anomalies appear over the mid-latitudes of the North Pacific around 35° N–65° N, indicating a strengthened AL. Meanwhile, significant positive SLP anomalies are seen over the high latitudes (Fig. 1a), suggesting a negative connection between the winter AL and the Arctic Oscillation (Thompson and Wallace 1998, 2000). In addition, notable positive SLP anomalies appear over the subtropical western North Pacific. The SLP anomalies in association with the winter AL index (Fig. 1a) are

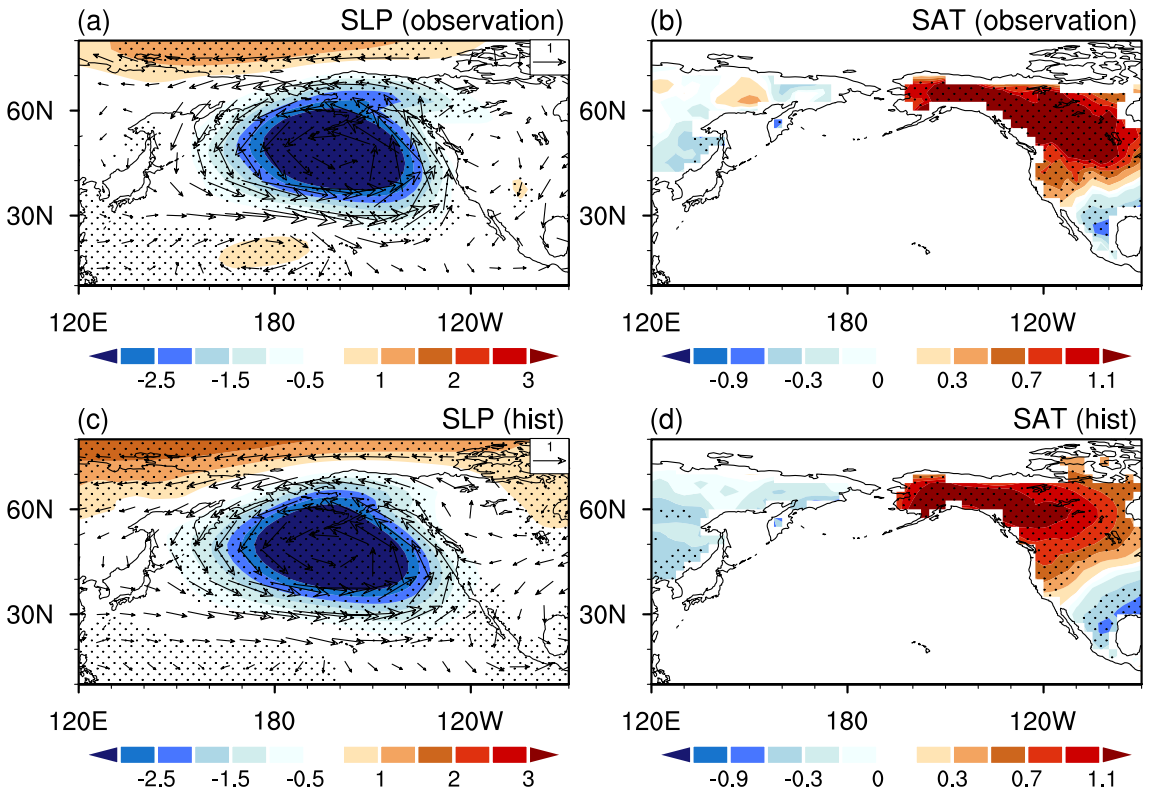

Fig. 1 Anomalies of winter (NDJFM-average) **a** SLP (hPa), 850-hPa winds (m s^{-1}), and **b** SAT (°C) regressed upon the normalized AL index in the simultaneous winter based on the observational data during period of 1948/49–2013/14. Stippling regions in **a**, **b** indicate SLP and SAT anomalies that are significant at the 95% confidence level, respectively. **c**, **d** As in **a**, **b**, but for the ensemble means of the 20 CMIP6 models over 1948/49–2013/14

consistent with previous studies obtained using various datasets (Song and Duan 2015; Yu and Kim 2011; Chen et al. 2020), indicating the robustness of these AL-related features. The MME of the CMIP6 models can well reproduce the observed AL pattern (Figs. 1c). The spatial correlation coefficient between the observed and MME SLP anomaly patterns reaches 0.98 over the region (15°–75° N and 120° E–120° W). Nevertheless, the MME pattern overestimates the AL-related positive SLP anomalies over the high latitudes and underestimates slightly the SLP anomalies over the subtropical central North Pacific (Fig. 1c versus Fig. 1a).

Figure 2a presents a Taylor diagram that compares the simultaneous SLP anomalies regressed upon the winter AL index over the region (15°–75° N, 120° E–120° W) in the 20 models with respect to the observational counterpart. Taylor diagram is constructed according to three statistics, including the spatial correlation between the observed and simulated patterns, the normalized standard deviation of spatial pattern, and the centered pattern root-mean-square (CRMS) difference (Taylor et al. 2012). The pattern correlations are higher than 0.8 (Fig. 2a), indicating that all the models can reasonably well simulate the observed spatial structure of the wintertime AL. However, there exists a large spread in the normalized standard deviation with values ranging from 0.8 to 1.4. The difference among individual models is mainly seen over the AL center (not shown). The CRMS ranges from 0.24 to 0.63 (Fig. 2a). The MME has a better capability than most models in reproducing the pattern standard deviation (the MME standard deviation is 1.07), pattern correlation (the MME pattern correlation is 0.98), and CRMS (the MME CRMS is 0.23) of the winter AL (Fig. 2a).

Figures 1b, d show regression maps of simultaneous SAT anomalies onto the normalized winter AL index in the observation and MME of the 20 models, respectively. In the observation, corresponding to a positive AL phase, pronounced positive SAT anomalies extend from Alaska southeastward to central Canada and the northwestern US. The anomalous southerly winds to the eastern side of the pronounced negative SLP anomalies (Fig. 1b) bring warm and wet air northward from the lower latitudes, leading to SAT increase over the above-mentioned regions. Meanwhile, negative SAT anomalies are seen over most parts of Mexico and the southeastern US. Several patches of significant SAT anomalies can also be seen over East Asia (Fig. 1b). The MME of the 20 models has a good performance in capturing the observed AL-related SAT pattern (cf. Fig. 1d with

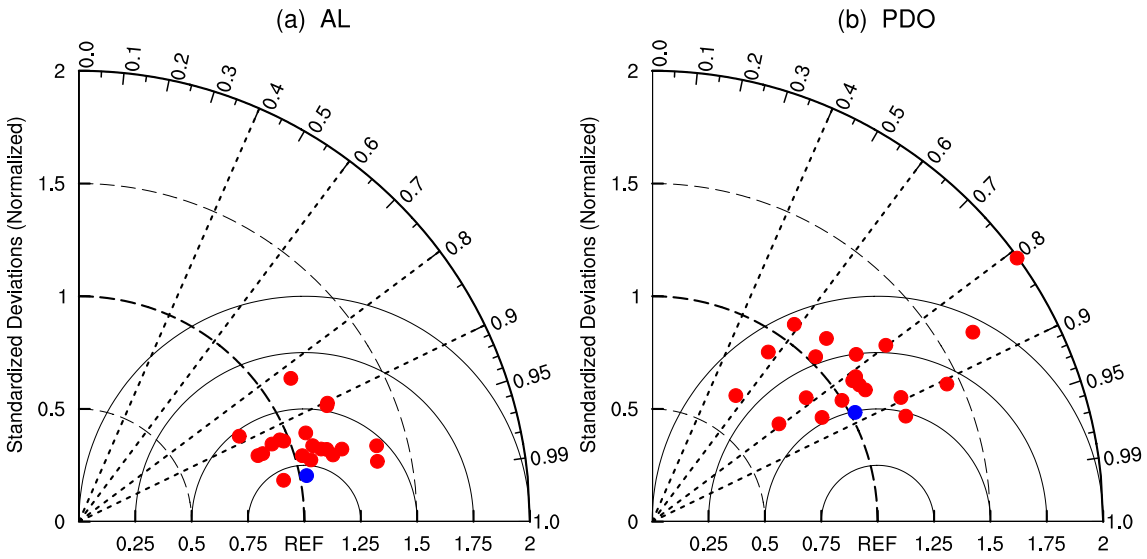

Fig. 2 **a** Taylor diagram of winter SLP anomalies regressed upon the winter AL index over the region (15°–75° N and 120° E–120° W) in historical simulations with respect to the observational counterpart. **b** Taylor diagram of winter SST anomalies regressed upon the winter PDO index over the region (30° S–60° N, 120° E–120° W) in historical simulations with respect to the observational counterpart. The blue dot indicates the ensemble mean result

Fig. 1b). However, negative SAT anomalies in the MME cover wider areas over Eurasia and shift northward compared to those in the observations. In addition, the MME pattern tends to overestimate the negative SAT anomalies over the southeastern US, whereas the center of positive SAT anomalies over North America shifts slightly northward.

Next, we examine the connection of the winter AL with Pacific SSTs. As would be expected, an El Niño-like pattern is seen in the tropical Pacific in the observations (Fig. 3a). Previous studies demonstrated that ENSO events influence the AL via a PNA-like atmospheric teleconnection (Wang et al. 2000; Alexander et al. 2002; Yu and Kim 2011). In particular, the strength of the winter AL is stronger (weaker) than normal when an El Niño (a La Nina) event appears in the tropical Pacific. The MME of the 20 models well captures this winter AL–ENSO connection (Fig. 3c, e). In particular, the correlation coefficients between the wintertime AL and Niño3 indices are significant at the 95% confidence level for all 20 models (Fig. 3e). Here, the Niño3 index is defined as the regional averaged SST anomalies over the region of 5° S–5° N and 90° W–150° W, which is generally used to represent the ENSO variability. The MME correlation coefficient between the winter AL and Niño3 indices is 0.52, close to that in the observation (0.51) (Fig. 3e).

The wintertime AL-related SST anomalies in the extratropical North Pacific bear a close resemblance to the positive phase of the PDO pattern (Mantua et al. 1997; and described below) in both the observation and MME, with significant negative SST anomalies in the central North Pacific, accompanied by positive SST anomalies along the North American western coastline (Fig. 3a, c). In fact, studies have demonstrated that AL is an important stochastic atmospheric forcing of the PDO (Latif and Barnett 1996; Pierce et al. 2001). The correlation coefficients between the winter AL and PDO indices are also significant at the 95% confidence level for all the models (Fig. 3f). The MME correlation coefficient of the AL–PDO relation reaches 0.6, slightly lower than that in the observation (0.7).

We have also evaluated the performance of these models in capturing the internal PDO pattern. Figure 3b, d display regression maps of simultaneous SST anomalies onto the winter PDO index in the observation and MME of the 20 models, respectively. Corresponding to a positive PDO phase, the SST anomalies feature a broad horseshoe shape in the Pacific basin, with cold anomalies centered over the mid-latitude North Pacific surrounded by warm anomalies extending off the west coast of North America to the tropical Pacific (Fig. 3b). The MME can reasonably well reproduce the observed SST pattern in association with the PDO index (Fig. 3d). The pattern correlation coefficients between the PDO-related simulated and observed SST anomalies are higher than 0.56 over the Pacific basin (30° S–60° N, 120° E–120° W) for all 20 models (Fig. 2b). The MME of the pattern correlation is 0.88, the mean pattern standard deviation is 1.02, and the mean CRMS is 0.5 (Fig. 2b).

Overall, the above results indicate that the CMIP6 models considered can reasonably well simulate the observed winter AL and PDO patterns, as well as the associations of the winter AL variability with the ENSO, PDO, and Eurasian and North American SAT anomalies.

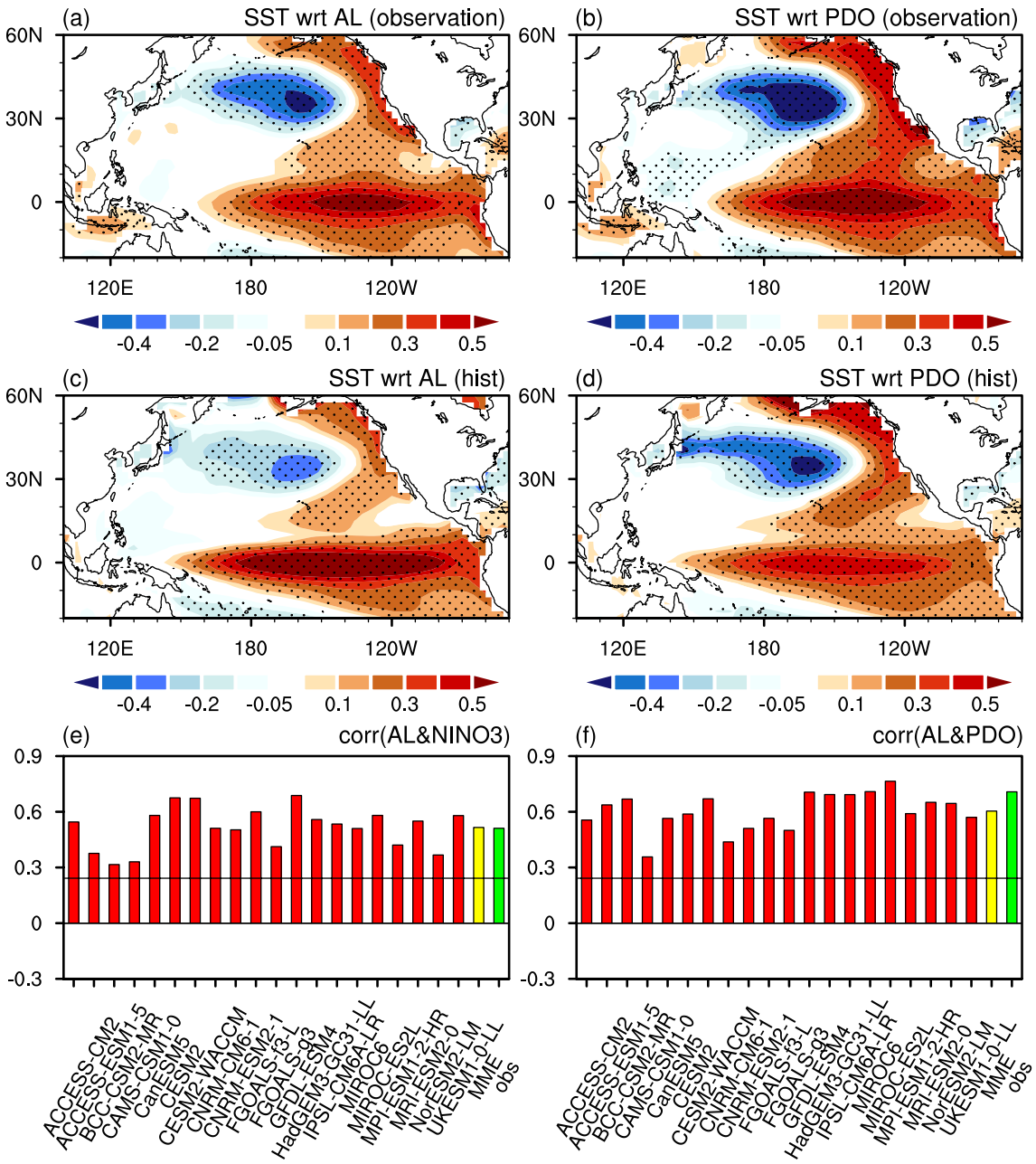

Fig. 3 Winter SST anomalies (°C) regressed upon the normalized winter **a** AL and **b** PDO index based on the observational data during the period of 1948/49–2013/14. **c**, **d** As in **a**, **b**, but for the ensemble mean of the 20 models over 1948/49–2013/14. Stippling regions in **a**–**d** indicate the SST anomalies significant at the 95% confidence level. Correlation coefficients of the winter AL index with the simultaneous winter **e** Niño3 and **f** PDO index for the period of 1948/49–2013/14. Yellow and green bars represent the ensemble means of the 20 CMIP6 models and observations, respectively. The horizontal line in **e**–**f** indicates the correlation coefficient significant at the 95% confidence level

3.2 NPO

Here we evaluate the model performance in simulating the winter NPO pattern and the NPO associated SAT and SST anomalies. The NPO pattern features a meridional dipole structure of SLP anomalies over the northern extratropics. A positive NPO phase is characterized by above-normal SLP over the subtropics and below-normal SLP extending from the Russian Far East to northwestern Canada (Fig. 4a). The MME of the 20 models well captures the observed NPO pattern, in particular, with a relatively stronger amplitude of SLP anomalies in the northern center of action than the southern center (cf. Fig. 4c with 4a). The pattern correlation coefficients of the SLP anomalies over the extratropical

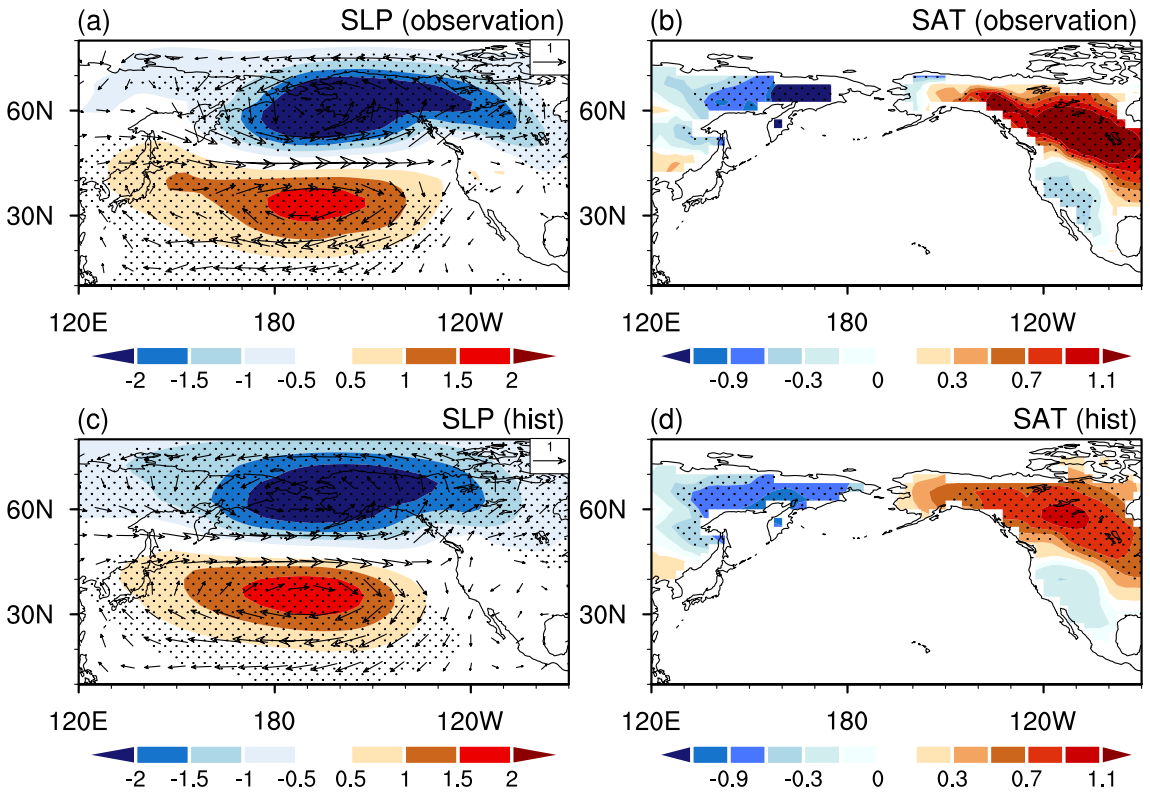

Fig. 4 Anomalies of winter (NDJFM-average) **a** SLP (hPa), 850-hPa winds (m s^{-1}), and **b** SAT (°C) regressed upon the normalized NPO index in the simultaneous winter based on the observational data during period of 1948/49–2013/14. Stippling regions in **a**, **b** indicate SLP and SAT anomalies significant at the 95% confidence level, respectively. **c**, **d** As in **a**, **b**, but for the ensemble means of the 20 CMIP6 models over 1948/49–2013/14

North Pacific (15°–75° N and 120° E–120° W) between each model and the observed are higher than 0.75, with a value of 0.95 between the MME and observed (Fig. 5a). Hence, the CMIP6 models can reasonably well simulate the winter NPO pattern.

The winter NPO-related SAT anomalies over Eurasia and North America are generally similar between the observations and MME (Fig. 4b, d). Corresponding to a positive NPO phase, there are below-normal SAT over the Russian Far East, the southwest US and northwest Mexico and above-normal SAT extending from eastern parts of Alaska southeastward to the Great Lakes. In comparison, the positive center of action over North America tends to shift northward and has a smaller amplitude in the MME compared to the observed. In addition, unlike that seen in the observed, the negative SAT anomalies over northwestern Mexico and the southwestern US in the MME cannot pass the 95% confidence level (Fig. 4d). These relatively weak SAT anomalies in the MME are likely due to the large divergence among the 20 models.

We then examine the winter NPO-associated SST anomalies. Previous studies indicated that NPO has a close relation with the second EOF mode of SST anomalies in the extratropical North Pacific (i.e., the Victoria Mode) (Bond et al. 2003; Ding et al. 2015) as well as the ENSO-like SST anomalies in the tropical central-eastern Pacific (Horel and Wallace 1981; Pak et al. 2014; Chen and Song 2018). It is suggested that the VM formation is largely forced by the NPO associated atmospheric anomalies via modulating the relevant surface heat fluxes (Bond et al. 2003; Ding et al. 2015). On the other hand, ENSO could exert impacts on the NPO variability via atmospheric teleconnections (Horel and Wallace 1981; Pak et al. 2014). Hence in the observations (Fig. 6a), the winter NPO-related SST anomalies exhibit a VM-like tripolar SST anomaly pattern in the extratropical North Pacific, with SST warming extending from the western North Pacific eastward to the central North Pacific along 20°–30° N, accompanied by SST cooling in the mid-latitude North Pacific and subtropical central North Pacific. In the tropics, an El Niño-like pattern can be seen, with significant warming in the tropical central-eastern Pacific and cooling in the tropical western Pacific (Fig. 6a). The correlation coefficient between the NPO and VM (Niño3) indices is 0.58 (0.35), significant at the 95% confidence level (Fig. 6e, f, green bars).

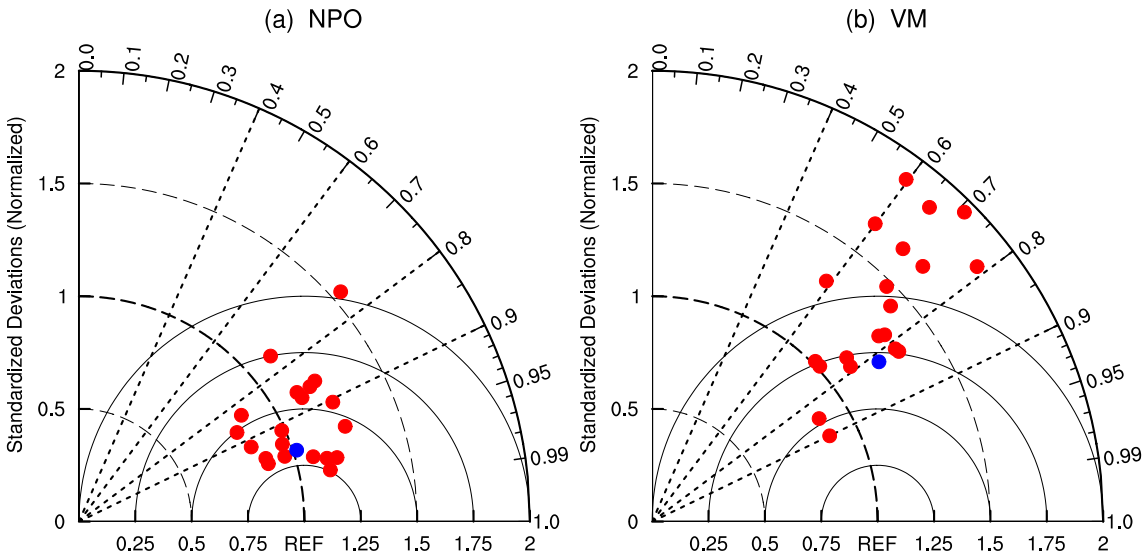

Fig. 5 **a** Taylor diagram of winter SLP anomalies regressed upon the winter NPO index over the region (15°–75° N and 120° E–120° W) in historical simulations with respect to the observational counterpart. **b** Taylor diagram of winter SST anomalies regressed upon the winter VM index over the region (10°–60° N, 120° E–120° W) in historical simulations with respect to the observational counterpart. The blue dot indicates the ensemble mean result

The MME can reasonably well capture the winter NPO-related SST pattern in the extratropical North Pacific (Fig. 6c). The correlation coefficient between the NPO and VM indices in the MME is 0.64 (Fig. 6f, yellow bar), slightly higher than that in the observation (0.58). In addition, all the models considered show significant connections between the NPO and VM indices (Fig. 6f). It should be mentioned that we have also examined the capability of the models in simulating the winter VM (Fig. 6b, d), as defined in Sect. 2. The pattern correlations of the VM-related SST anomalies in the extratropical North Pacific (10°–60° N, 120° E–120° W) are larger than 0.59 between the observed and the 20 models (Fig. 5b). This suggests that all the models can reasonably well reproduce the observed VM pattern. A comparison of Figs. 2a, 5a with Figs. 2b, 5b further indicates that the 20 models have a better performance in simulating the two dominant modes of atmospheric variability over the North Pacific compared to the SST counterparts.

The NPO-related SST anomalies in the tropical Pacific cannot pass the 95% confidence level in the MME (Fig. 6c), which is due to a large spread of the winter NPO–ENSO connection across the 20 models (Fig. 5b). In particular, only 7 models (i.e. CAMS-CSM1-0, CNRM-CM6-1, FGOALS-f3-L, MIROC6, MIROC-ES2L, MPI-ESM1-2-HR, NorESM2-LM) can produce significant connections between the winter NPO and Niño3 indices (Fig. 6e). This implies that the tropical ENSO related SST anomalies have little contribution to the NPO variability in most models.

3.3 Factors for the large spread of the winter NPO–ENSO relation

The above analysis indicates that there exists a large diversity of the winter NPO–ENSO relationship across the 20 models. Possible factors leading to this large spread of the NPO–ENSO relation are discussed in this subsection. We select the 7 models that produce significant winter NPO–ENSO connections as Group A models (Fig. 6e). The other 13 models, which produce weak NPO–ENSO relations, are considered as Group B models (Fig. 6e). Figure 7 compares the ensemble means of winter SST, SLP, SAT anomalies regressed upon the winter NPO index for the two groups. The winter NPO-related SST anomalies in the extratropical North Pacific are similar to the VM for both Group A and Group B models, consistent with the fact that all the 20 models produce significant winter NPO–VM connections (Fig. 6f). However, an El Niño-like SST pattern is only seen in the ensemble mean of the Group A models (Fig. 7a), whereas the SST anomalies are weak in the tropical Pacific for the Group B models (Fig. 7b). Meanwhile, the NPO associated SLP anomalies over the tropical North Pacific shift considerably southwestward in the ensemble mean of the Group A models compared to that of the Group B models (Fig. 7c, d), resulting in the difference in tropical zonal pressure gradients between the two groups. In addition, significant positive SLP anomalies can be seen over the tropical western North Pacific for the Group A models. Meanwhile, the amplitude of the negative SLP anomalies around Alaska and Bering Strait is much larger in Group A

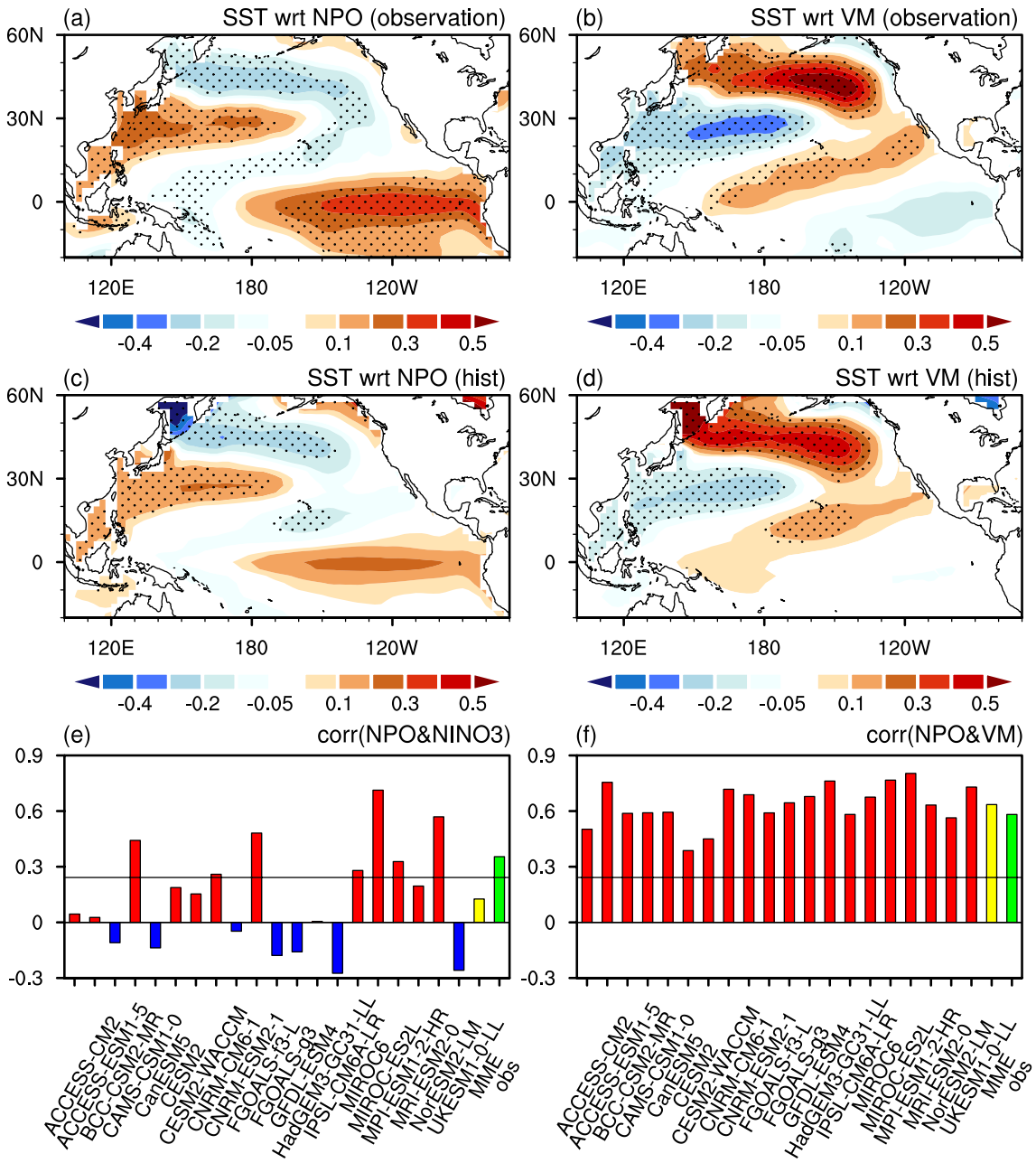

Fig. 6 Winter SST anomalies (°C) regressed upon the normalized winter **a** NPO and **b** VM index based on the observational data during the period of 1948/49–2013/14. **c**, **d** As in **a**, **b**, but for the ensemble mean of the 20 models over 1948/49–2013/14. Stippling regions in **a**–**d** indicates SST anomalies significant at the 95% confidence level. Correlation coefficients of the winter NPO index with the simultaneous winter **e** Niño3 and **f** VM index for the period of 1948/49–2013/14. Yellow and green bars represent the ensemble means of the 20 CMIP6 models and observations, respectively. Horizontal line in **e**, **f** indicates the correlation coefficient significant at the 95% confidence level

than Group B models. Correspondingly, the NPO-related SAT anomalies over North America and the Russian Far East are larger and shift slightly eastward in the Group A models than in the Group B models (Fig. 7e, f). In addition, significant positive SAT anomalies are found over south China for the Group A models but not for the Group B models. For the Group A mean, the significant positive SLP anomalies over the tropical western North Pacific are accompanied by anomalous southerly winds to its west side (not shown), which contribute to the formation of the positive SAT anomalies over south China via bringing warmer air northward.

In the following, we further examine the factors responsible for the diversity of the winter ENSO–NPO connection

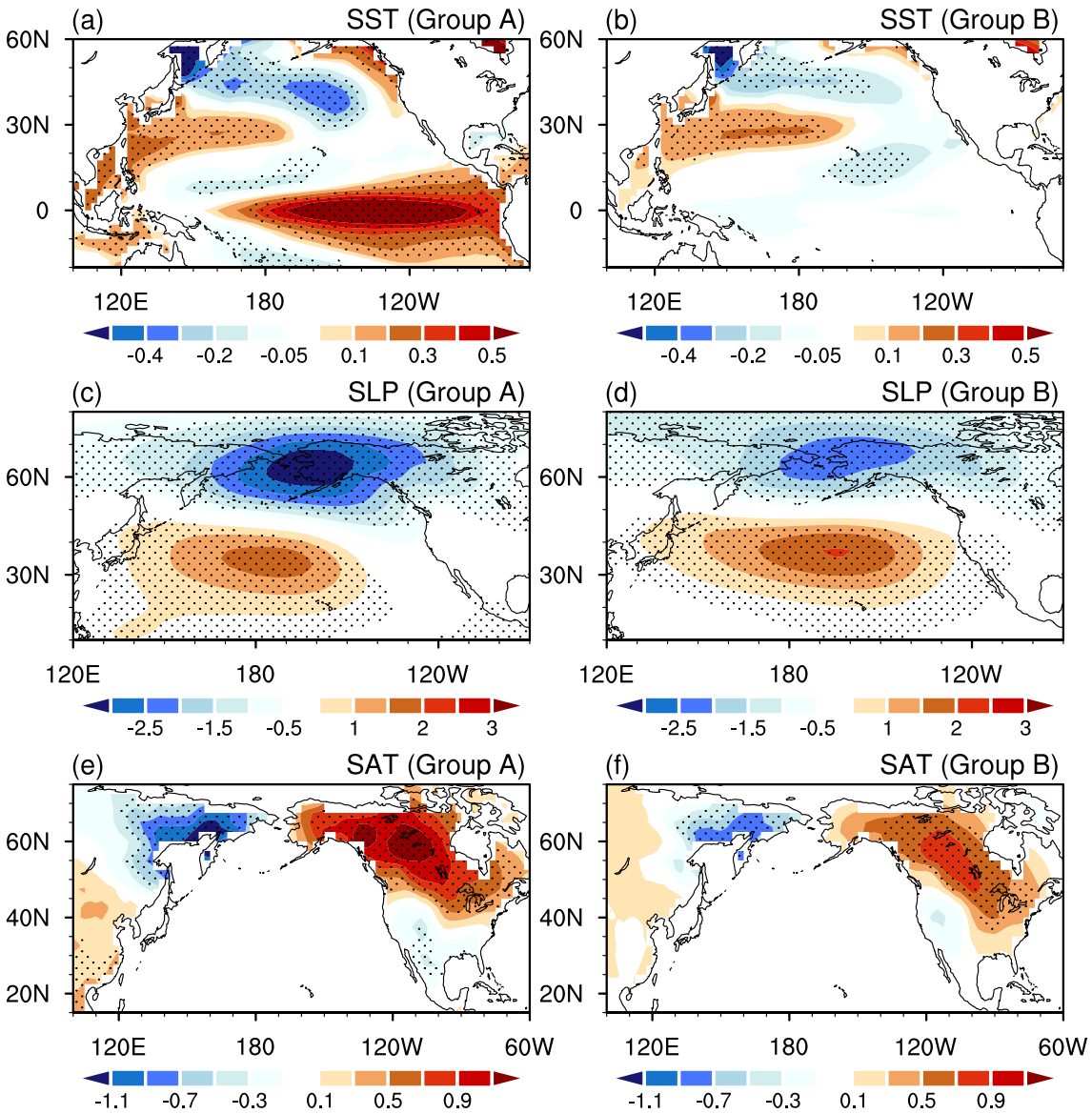

Fig. 7 Ensemble means of winter **a**, **b** SST (unit: °C), **c**, **d** SLP (unit: hPa), and **e**, **f** SAT (unit: °C) anomalies regressed upon the normalized winter NPO index for (left) Group A models and (right) Group B models. Stippling regions indicate anomalies significant at the 95% confidence level. Here, 7 models are selected as Group A models that produce significant winter NPO–ENSO connections. The other 13 models, which produce weak NPO–ENSO relations, are considered as Group B models. Detailed definitions of the Group A and B models are provided in the text

among the 20 models. First, we examine models' performances in simulating the seasonal evolution and phase locking of the ENSO. Figure 8a shows evolutions of SST anomalies in the Niño3 region from the preceding to the following winter regressed upon the winter Niño3 index during 1948/49–2013/14 for the ensemble means of the (red line) Group A models and (blue line) Group B models. The evolutions of SST anomalies in the Niño3 region are similar between the two model Groups and are in good agreement with the observed as reported in previous studies (e.g. Wang et al. 2000). Figure 8b displays standard deviations of the monthly Niño3 index during 1948/49–2013/14 for the ensemble means of (red line) Group A models and (blue line) Group B models. The standard deviations have high values during boreal winter for both the Group A and B models, suggesting the two Group models can well capture the winter phase locking of the ENSO evolution as in the observed (Wang et al. 2000). The similarities between the two groups also indicate that the ability of the models considered in simulating the close winter ENSO–NPO relation is not likely due to its performance in capturing the phase locking and seasonal evolution of ENSO events. The

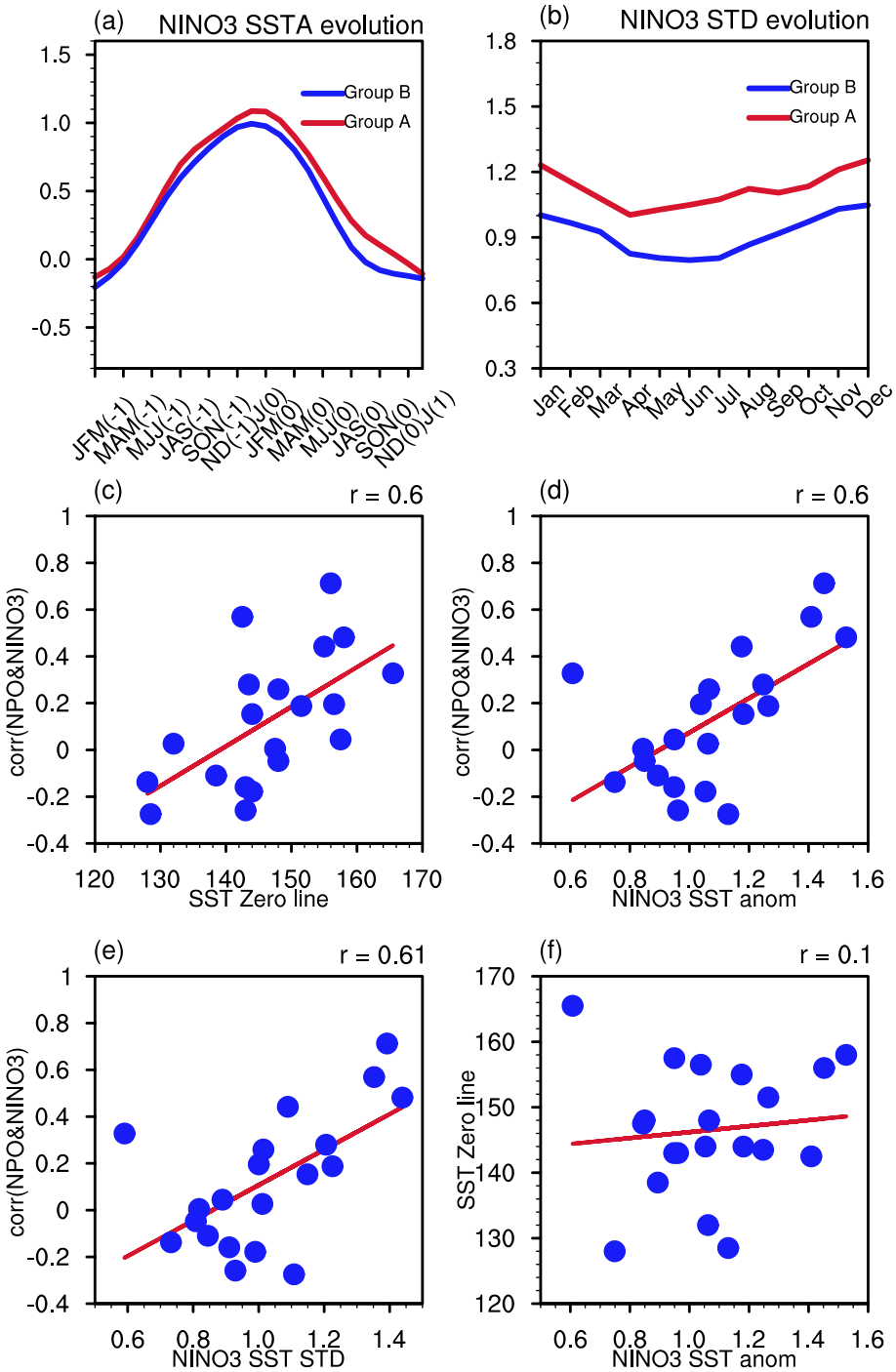

Fig. 8 **a** Evolutions of SST anomalies (°C) from preceding to following winter regressed upon the winter Niño3 index for the ensemble means of Group (red) A and (blue) B models. **b** Seasonal cycle of standard deviation (°C) of the Niño3 index for the ensemble means of Group (red) A and (blue) B models. Scatter plots of winter NPO–Niño3 correlation coefficient against **c** longitudinal location of the 0 °C isoline of winter SST anomalies over equatorial western Pacific, **d** winter SST anomalies averaged in the Niño3 region regressed upon the winter Niño3 index, and **e** standard deviation of the winter Niño3 index during 1948/49–2013/14 among the 20 models. **f** Scatter plots between longitudinal location of the 0 °C isoline of winter SST anomalies over equatorial western Pacific against winter SST anomalies averaged in the Niño3 region regressed upon the winter Niño3 index

differences of the SST anomalies and standard deviation of the Niño3 index in winter between the two groups will also be discussed later.

Figure 9 displays the ensemble means of the simultaneous SST, precipitation, and SLP anomalies regressed upon the winter Niño3 index for the Group A and Group B models. The ensemble mean of the SST anomaly pattern in the Pacific in the Group A models tends to shift slightly eastward compared to the counterpart in the Group B models (Fig. 9a, b). In particular, the isolines of 0 °C in the equatorial western Pacific are located around 145° E and 135° E, respectively, in the Group A and Group B models (Fig. 9a, b). Correspondingly, the regions of the maximum positive precipitation anomalies in the tropical Pacific and associated atmospheric circulation also shift eastward in the Group A models than in the Group B models (Fig. 9c–f). For the Group B models, the spatial pattern of the Niño3-related SLP anomalies over the North Pacific (Fig. 9f) seems to

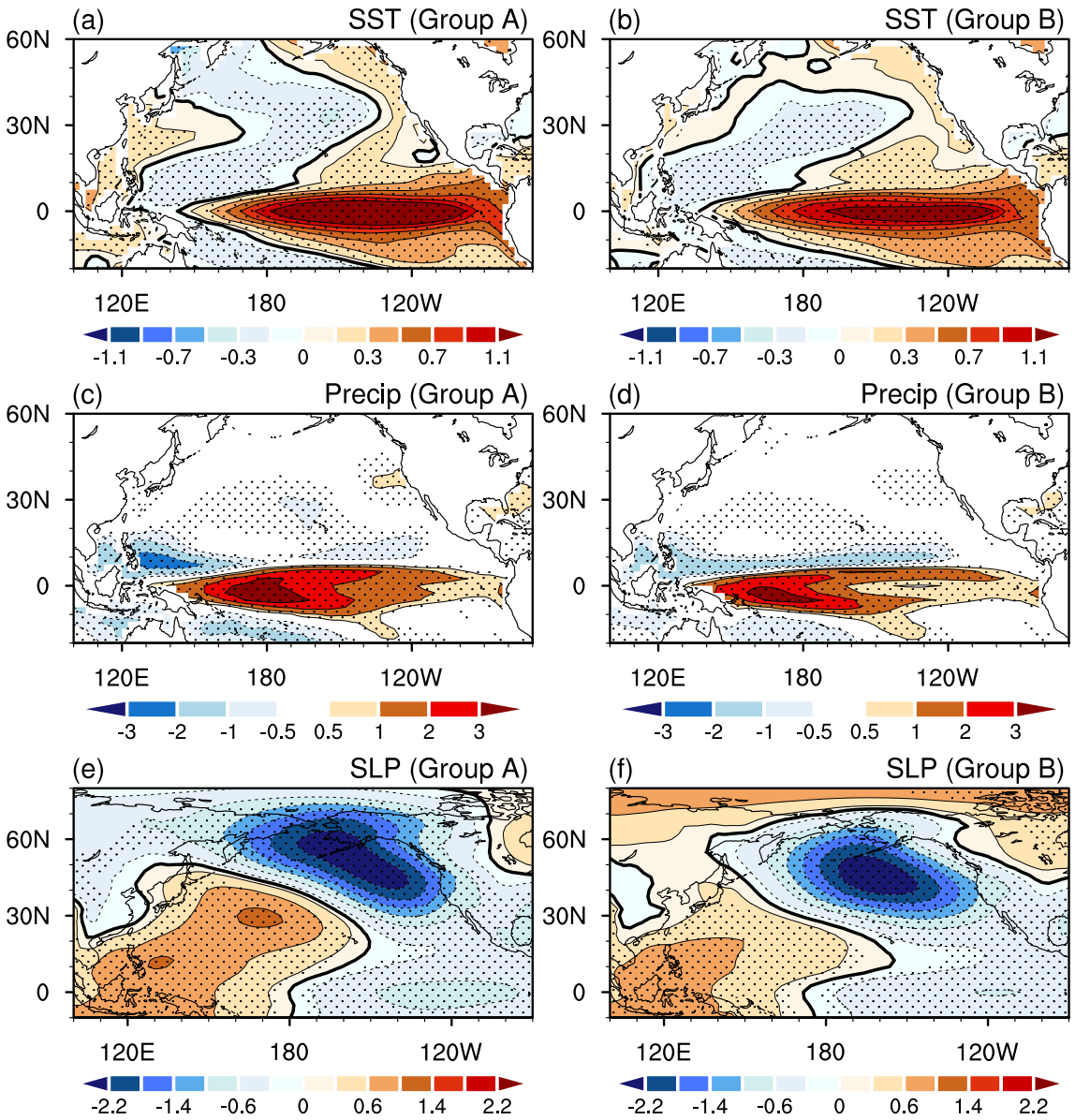

Fig. 9 Ensemble means of winter **a**, **b** SST (unit: °C), **c**, **d** precipitation (unit: mm day^{-1}), and **e**, **f** SLP (unit: hPa) anomalies regressed upon the normalized winter Niño3 index for (left) Group A models and (right) Group B models. Stippling regions indicate anomalies significant at the 95% confidence level. Here, 7 models are selected as Group A models that produce significant winter NPO–ENSO connections. The other 13 models, which produce weak NPO–ENSO relations, are considered as Group B models. Detailed definitions of the Group A and B models are provided in the text

be spatially orthogonal to the SLP anomaly pattern associated with the winter NPO (Fig. 8d). As such, the winter ENSO–NPO relation is weak for the Group B models. By contrast, the eastward movement of the SLP anomaly pattern for the Group A models, which is due to the correspondingly eastward shifted SST and precipitation anomalies in the tropical Pacific, leads to a significant contribution of the winter ENSO to the NPO-associated atmospheric circulation anomalies. The above analysis hence indicates that the large spread of the winter ENSO–NPO relation among the models is partly attributed to the divergence of the zonal locations of the tropical SST and atmospheric convection anomalies. Previous studies have demonstrated that the spatial structure of atmospheric teleconnections over the North Pacific is quite sensitive to the zonal location of the tropical forcings (Trenberth et al. 1998; Barsugli and Sardeshmukh 2002; Cherchi et al. 2012; Ji et al. 2014; Jo et al. 2015; Soulard et al. 2019). In particular, atmospheric teleconnections induced by the tropical forcing would shift westward (eastward) if the center of the tropical forcing is located more westward (eastward)

(Jo et al. 2015; Soulard et al. 2019). Figure 8c displays a scatter plot between the winter NPO–Niño3 correlation coefficients against zonal locations of the 0 °C isoline of winter SST anomalies in the equatorial western Pacific related to ENSO among the 20 models. The correlation coefficient between the two quantities in Fig. 8c reaches 0.6, significant at the 99% confidence level. This further confirms the above result that changes in the zonal location of the ENSO-associated tropical SST anomalies significantly modulate the NPO–ENSO relation.

The intensities of the Niño3-related SST, precipitation, and SLP zonal gradient anomalies along the tropical Pacific tend to be stronger in the Group A than Group B models (Fig. 9), consistent with those shown in Fig. 8a, b. Figure 8d, e further present scatter plots of the winter NPO–Niño3 correlation coefficients against the ENSO-related SST anomalies averaged in the Niño3 region, and against standard deviations of the Niño3 index, respectively, among the 20 models. Based on these relationships, a model with a strong amplitude of the winter ENSO tends to produce a high correlation between the winter NPO and ENSO. This also suggests that the spread in the NPO–ENSO relations among the 20 models is partly related to the divergence of the ENSO intensity. In addition, it is noted that the spread in the ENSO intensity has a weak relation with the spread in the zonal shift of the SST anomaly pattern in the tropical Pacific (Fig. 8f). This implies that changes in the amplitude of ENSO and zonal shift of the ENSO-related SST anomaly pattern tend to be two independent factors contributed to the spread of the winter ENSO–NPO relation among the models. Nevertheless, the physical process responsible for the modulation of the ENSO's amplitude on the winter ENSO–NPO connection remains to be explored.

4 Projected changes in the winter AL and NPO

In this section, we explore projected changes of the winter AL and NPO patterns and their associations with the ENSO, PDO and VM in a warming climate. Here, projected changes are defined as state differences between the periods of 2033/34–2098/99 and 1948/49–2013/14. First, we analyze changes in the spatial structures and amplitudes of the winter AL and NPO. We then examine projected changes in the associations of the winter AL with the PDO and ENSO as well as the NPO–ENSO/VM connection. Finally, we discuss the possible factors responsible for a large uncertainty of projected changes of the AL–ENSO relationship.

Figure 10a, c display the ensemble means of simultaneous SLP and 850-hPa wind anomalies regressed upon the winter AL and NPO indices, respectively, over 2033/34–2098/99. The spatial patterns of the SLP anomalies in association with the winter AL and NPO variability over 2033/34–2098/99 are pretty similar to the corresponding patterns over 1948/49–2013/14 (Fig. 10a, c vs Figs. 1c, 4c), with pattern correlations of 0.99 over the North Pacific (20°–70° N, 160° E–120° W) between the two periods. Correspondingly, the winter AL/NPO-related SAT anomalies over Eurasia and North America over 2033/34–2098/99 (Fig. 10b–d) are also similar to those over 1948/49–2013/14. Figure 11 shows projected changes in the locations of the centers of the winter AL and NPO in each model, and their MMEs. Consistent with the results obtained from CMIP5 (Chen et al. 2018), the MME of the 20 CMIP6 models considered in this study projects a northward shift of the winter AL (Fig. 11a). For the individual model, nine models show a poleward movement of the center of the winter AL in the future, with amplitudes larger than 2.5 degrees of latitude. One model shows an equatorward shift of the winter AL center by 2.5 degrees of latitude in a warming climate. The meridional locations of the center of the AL remain the same in other ten models (Fig. 11a). The projected change in the zonal location of the AL is weak due to a large spread among the models (Fig. 11b). For the MME, the centers of the NPO's north and south poles are projected to shift equatorward of about one degree of latitude. Compared to the meridional location, there exist much larger uncertainty in the projected change of the zonal movement of the NPO (Fig. 11f, d versus Fig. 11c, e).

We then examine projected changes in the intensity of the winter AL and NPO. Here, the amplitude of the winter AL for each model is defined as the absolute value of its minimum of the AL-associated SLP anomalies over the North Pacific. The amplitude of the southern (northern) pole of the winter NPO is considered as the absolute value of the maximum (minimum) of the NPO-associated SLP anomalies over the subtropical (mid-latitude) North Pacific. Subsequently, the amplitude of the NPO is defined as the sum of the amplitudes of its southern and northern poles. The AL and NPO amplitudes we defined here indicate the SLP anomalies in association with the interannual AL and NPO variability. Figure 12a shows the differences of the AL amplitude between 2033/34–2098/99 and 1948/49–2013/14 in the 20 models and MME. There exists a large uncertainty in the projected changes of the winter AL amplitude. The AL amplitude increases in half of the models and decreases in the other half of models with climate warming (Fig. 12a). Similarity, large diversities across the 20 models are also apparent in the projected changes of the NPO amplitude, including comparable changes in the southern and northern poles of the NPO (Figs. 12b, d, f). Overall, there are no consensus on the projected changes of the intensities of the winter AL and NPO patterns, under the SSP2-RCP45 scenario, across the 20 models. Our preliminary analysis indicates that the spread in changes of the AL intensity has a close

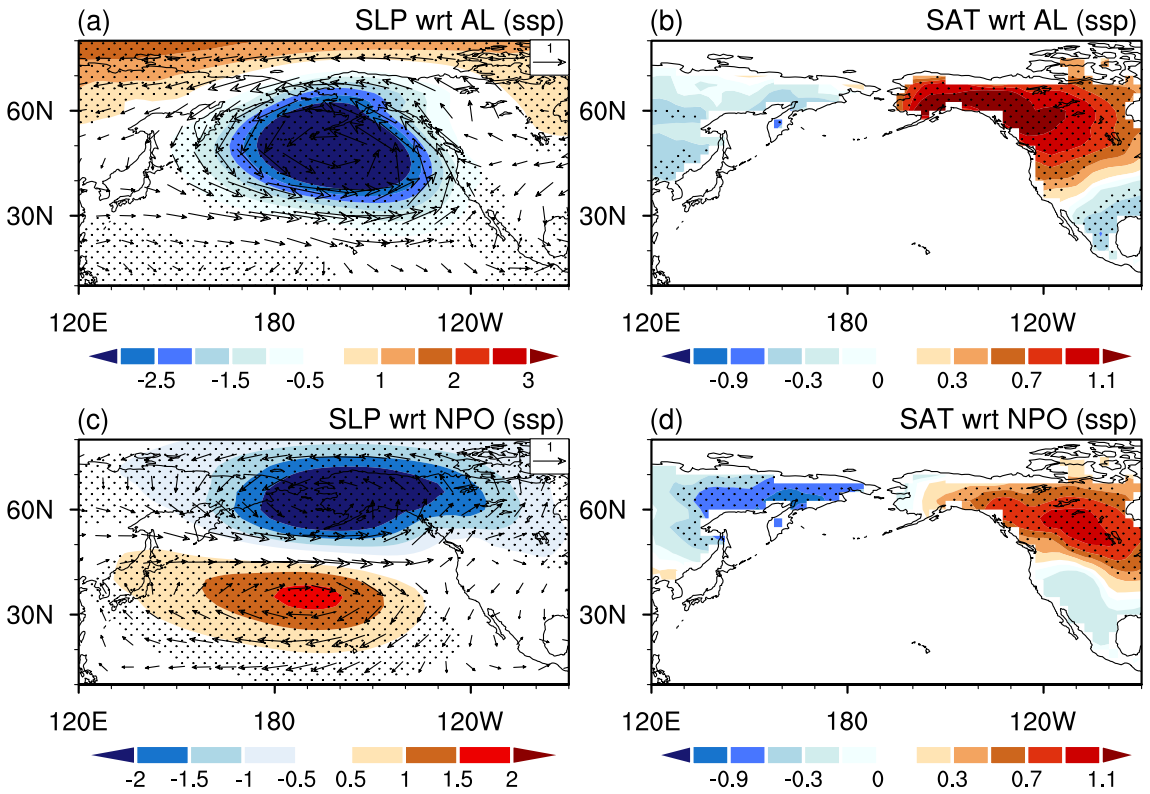

Fig. 10 SLP (hPa) and 850-hPa winds (m s^{-1}) anomalies in winter (NDJFM-average) regressed upon the normalized **a** AL and **c** NPO index in the simultaneous winter for the ensemble means of the 20 CMIP6 models over 2033/34–2098/99. **b**, **d** are as in **a**, **c**, but for the winter SAT anomalies (°C). Stippling regions in **a**, **c** and **b**, **d** indicate SLP and SAT anomalies, respectively, significant at the 95% confidence level

relation with that in changes in the ENSO-associated SLP anomalies over the mid-latitude North Pacific (Fig. 12e). Factors responsible for the large diversity of the NPO intensity remain to be explored.

Previous studies indicated that the winter AL intensity is projected to be strengthened in a warmer climate based on CMIP5 simulations (e.g., Gan et al. 2017 and references therein). Those studies mainly focused on long-term trends of the winter AL intensity, which is different from this study focusing on projected changes of the interannual AL variability. For comparison, we have examined projected changes in the winter AL intensity, which is generally defined as SLP anomalies averaged over the North Pacific (30°–65° N, 160° E–140° W) and denoted as the North Pacific index (NPI; Trenberth and Hurrell 1994). Figure 12c shows the differences between the NPI means over 2033/34–2098/99 and 1948/49–2013/14 in each model and the MME. The winter AL intensity increases in 17 of the 20 models as well as in the MME (Fig. 12c). Hence, the CMIP6 models produce a strengthened winter AL intensity with global warming, consistent with CMIP5 model results.

Figure 13a, c display the correlation coefficients of the winter AL index with the winter Niño3 and PDO indices over 2033/34–2098/99 in each model and the MME. Under the warming climate, all the models and the MME produce significant correlations between the winter AL and Niño3 indices except for ACCESS-ESM1-5, as well as significant correlations between the winter AL and PDO indices. This suggests that the connections of the winter AL with the PDO and ENSO variability are still robust in a warming climate. It should be mentioned that the PDO and VM patterns over 2033/34–2098/99 (not shown) are similar to those over 1948/49–2013/14. In addition, the winter NPO still has a marked connection with the VM in all models during the warming climate (Fig. 13g). By contrast, the winter NPO–ENSO relations show a large spread over 2033/34–2098/99, with only 8 out of the 20 models displaying significant relations of the winter NPO with ENSO (Fig. 13b). Figure 14a, c, e show scatter plots of the winter NPO–ENSO correlation coefficients against the zonal locations of the 0 °C isoline of winter SST anomalies in the equatorial western Pacific, ENSO-related SST anomalies averaged in the Niño3 region, and standard deviations of the Niño3 index, respectively, among the 20 models over 2033/34–2098/99. It is clear that, similar to the historical simulation result, the large diversity of the winter

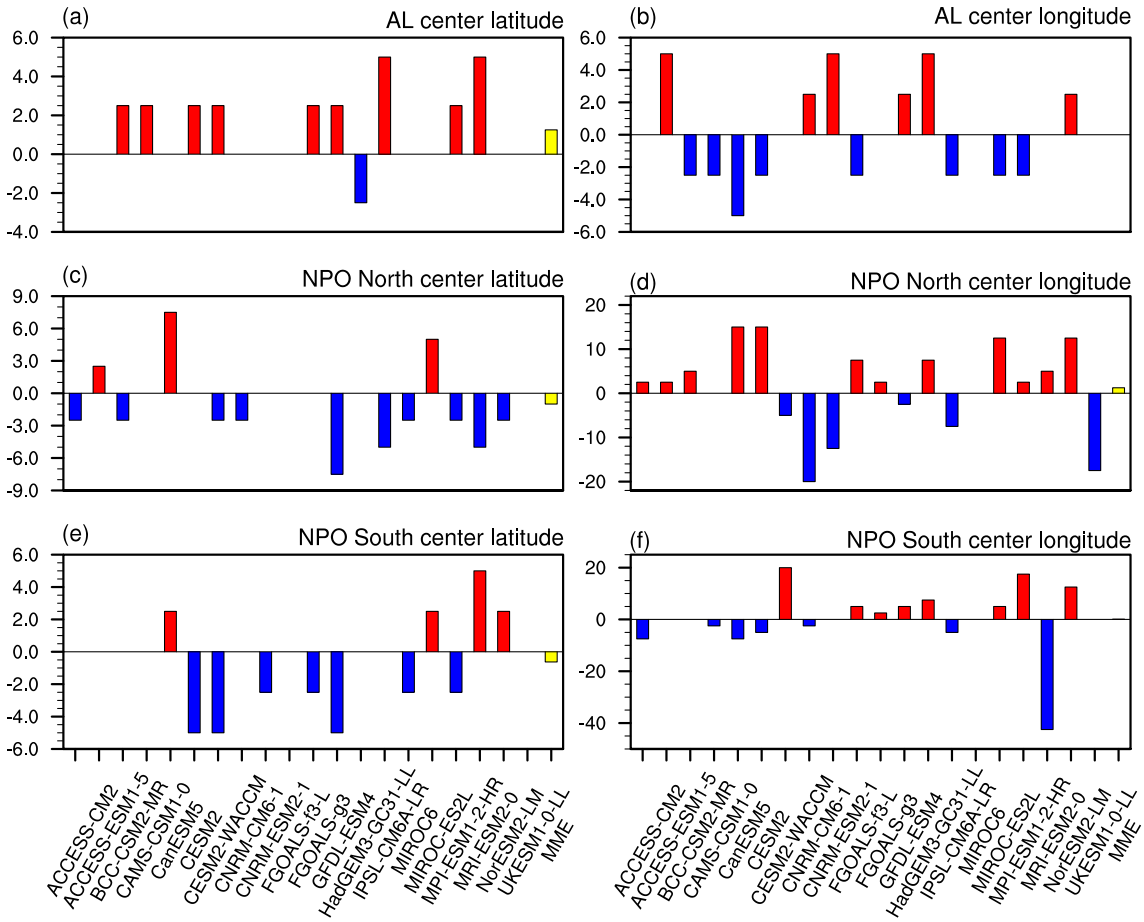

Fig. 11 Projected changes in the **a** meridional (degree of latitude) and longitudinal (degree of longitude) locations of the center of the winter AL. **c–f** Are as in **a**, **b**, but for northern and southern centers of the NPO, respectively. Projected changes are defined as the anomalies over 2033/34–2098/98 minus those over 1948/49–2013/14

NPO–ENSO relation in the warming climate is also closely related to spreads in the zonal location of the ENSO-related tropical SST anomaly pattern and the ENSO intensity (Fig. 14a, c, e).

Next, we examine projected changes in the connections of the winter AL with the ENSO and PDO as well as changes in the NPO–ENSO/VM relationship. Figures 13b (13d) displays the differences of the correlations between the winter AL and Niño3 (PDO) indices between 2033/34–2098/99 and 1948/49–2013/14 in the 20 models and MME. Figure 13f (13h) shows the corresponding result of correlations between the winter NPO and Niño3 (VM) indices. 10 models produce an increase of the winter AL–ENSO relation, whereas the other half of the models show a decrease of the relationship, and hence the MME of the AL–ENSO connections is pretty weak (Fig. 13b). 13 (7) out of the 20 models show an increase (a decrease) in the AL–PDO relation, and hence there is a weak positive AL–PDO connection in the MME (Fig. 13d). These suggest that there exist large uncertainties in the projected changes of the winter AL-associated SST anomalies in the Pacific basin, especially the AL–ENSO relationship. 17 out of the 20 models, as well as the MME, project a decrease of the winter NPO–VM relation (Fig. 13h). This suggests that the winter NPO–VM connection tends to be weakened in a warming climate. By contrast, there appears considerable uncertainty in the projection of the winter NPO–ENSO relation (Fig. 13f). A preliminary analysis indicates that the projected change in the winter NPO–ENSO relation is not related to the projected change in the ENSO intensity (Fig. 14d, f), but has a close connection with the change in the zonal position of the ENSO-related SST anomaly pattern (Fig. 14b). This suggests that the zonal movement of the SST anomaly pattern in the tropical Pacific plays a more important role in modulating the winter NPO–ENSO relation compared to the ENSO intensity in a warming climate. It should be noted that the NPO is an internal atmospheric variability mode over the North Pacific. Hence, the projection of the winter ENSO–NPO connection may also be related to the change

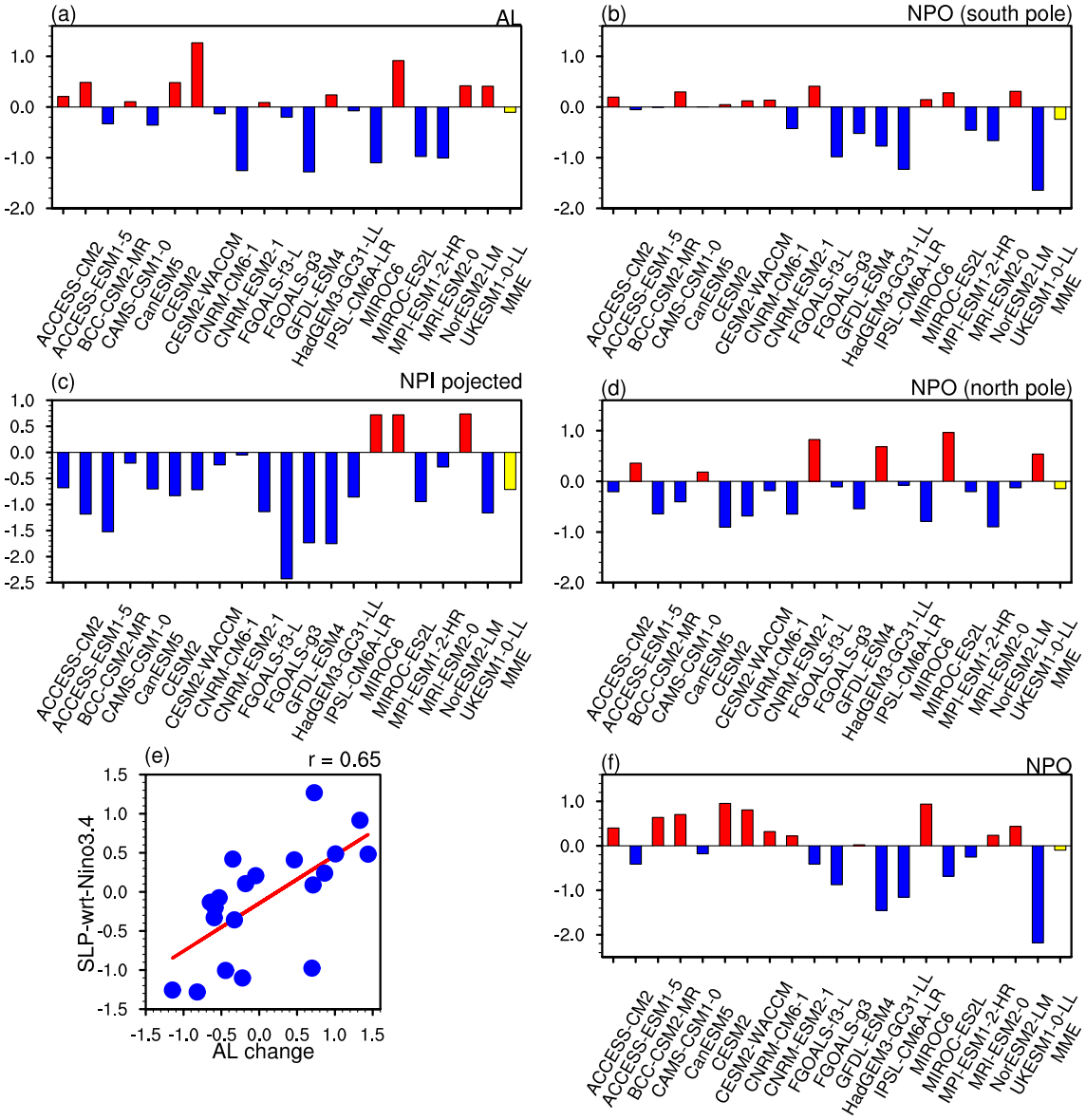

Fig. 12 Projected changes in the amplitudes (hPa) of **a** winter AL, **b** southern and **d** northern pole of winter NPO, and **f** NPO strength for the 20 models and their ensemble mean. Projected changes are defined as the anomalies over 2033/34–2098/98 minus those over 1948/49–2013/14. **c** Difference in the North Pacific index (NPI) between the periods of 2033/34–2098/98 and 1948/49–2013/14. NPI is defines as area-average SLP anomalies over 30°–65° N, 160° E–140° W, following Trenberth and Hurrell (1994). **E** A scatter plot between projected changes in the amplitude of the winter AL index against projected changes in the winter Niño3-related SLP anomalies averaged over the region (40°–60° N, 160° W–180°)

in mean state of the atmospheric circulation, which needs to be further investigated.

Finally, we discuss the possible factors responsible for the large spread of projected changes in the winter AL–ENSO connection by analyzing the models with large projected changes of the winter AL–ENSO relationship. Specifically, we compare the models with the projected changes of the AL–ENSO correlation higher than 0.1 (denoted as Group P models) to models with the correlation changes lower than − 0.1 (denoted as Group N models). The Group P involves 5 models, and Group N involves 6 models (Fig. 13b).

Figure 15a, c display the ensemble means of the SLP anomalies regressed upon the Niño3 index in winter for the Group P models over 1948/49–2013/14 and 2033/34–2098/99, respectively. Figure 15e shows the difference between the two ensemble means. Figure 15b, d, f are similar to those in Fig. 15a, c, e, respectively, but for the Group N models. For the Group P models, the winter Niño3-related SLP anomalies over the mid-latitude North

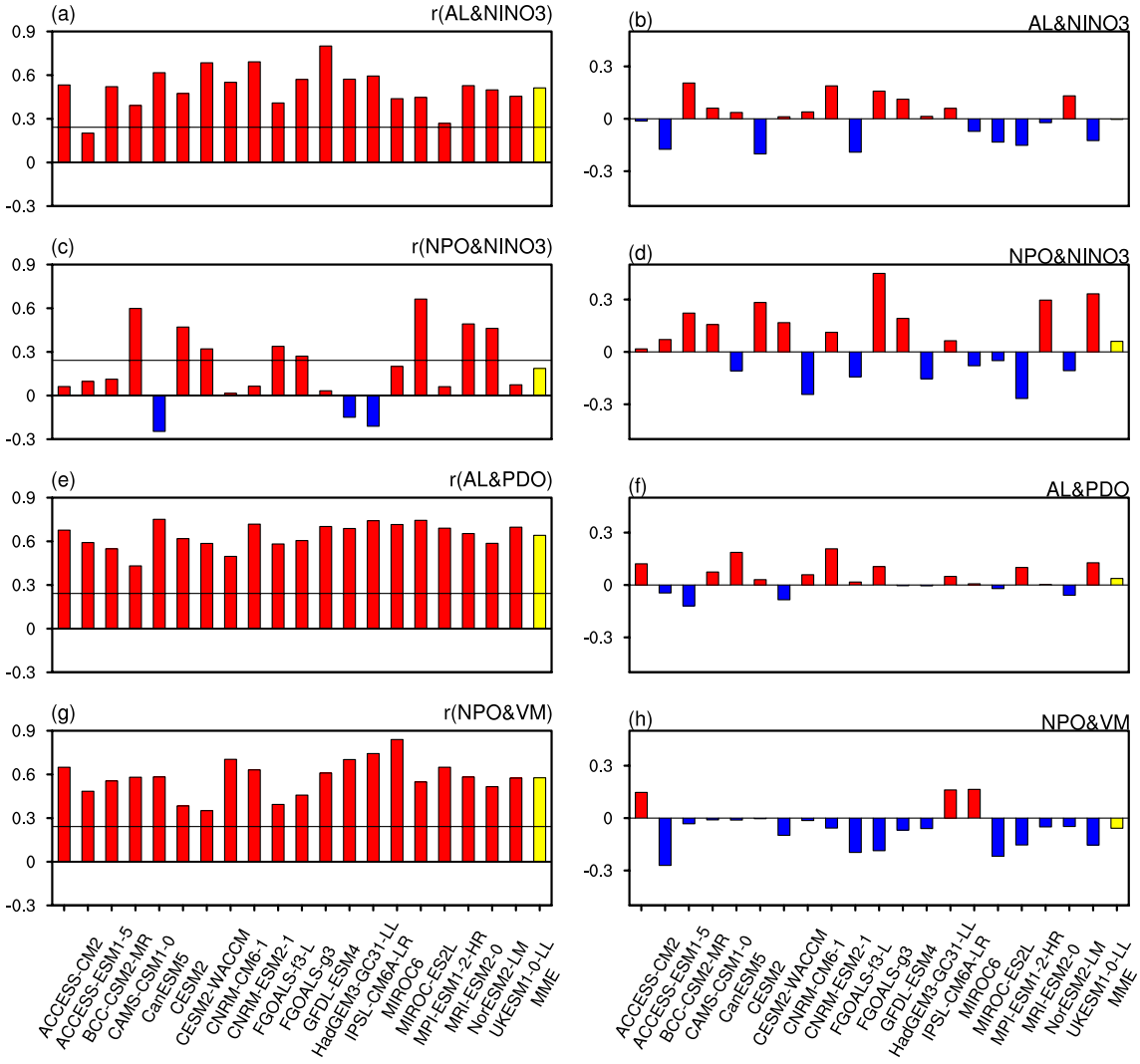

Fig. 13 Correlation coefficients of **a** the winter AL and Niño3 indices, **c** the winter NPO and Niño3 indices, **e** the winter AL and PDO indices, and **g** the winter NPO and VM indices for the 20 models and their ensemble means during 2033/34–2098/99. The horizontal line indicates the correlation coefficient significant at the 95% confidence level. Differences in the correlations of **b** the winter AL and Niño3 indices, **d** the winter NPO and Niño3 indices, **f** the winter AL and PDO indices, and **h** the winter NPO and VM indices between the periods of 2033/34–2098/99 and 1948/49–2013/14 for the 20 models and their ensemble means. Yellow bars indicate the ensemble means of the 20 models

Pacific are much stronger over 2033/34–2098/99 than over 1948/49–2013/14 (Fig. 15a, c), as clearly seen in the difference (Fig. 15e). This suggests a strengthened impact of the winter ENSO on the AL intensity. By contrast, the Group N models project a significant decrease in the ENSO-related negative SLP anomalies over the North Pacific (Fig. 15b, d, f), indicating a weakened influence of ENSO on the AL.

Previous studies have indicated that ENSO events exert impacts on the AL via tropical convection-induced atmospheric teleconnections (Hoskins and Karoly 1981; Trenberth et al., 1998; Luo et al. 2011). In addition, the strength of the ENSO-related atmospheric teleconnection over the North Pacific is closely correlated to the intensity of the tropical SST and precipitation anomalies induced by ENSO (Zhou et al. 2007; Chen et al. 2015, 2017; Chen et al. 2018). Figure 16a, b further show projected changes in the SST and precipitation anomalies, respectively, regressed upon the winter Niño3 index for the Group P models. Figure 16c, d display the corresponding changes for the Group N models. The Group P models produce an increase of SSTs in the tropical central-eastern Pacific (Fig. 16a). Correspondingly, significant increases of precipitation are projected in the tropical central-eastern Pacific (Fig. 16b), resulting in a strengthening of the ENSO-induced atmospheric teleconnection over the North Pacific and leading to an increase of the winter ENSO–AL connection (Fig. 15e). By contrast,

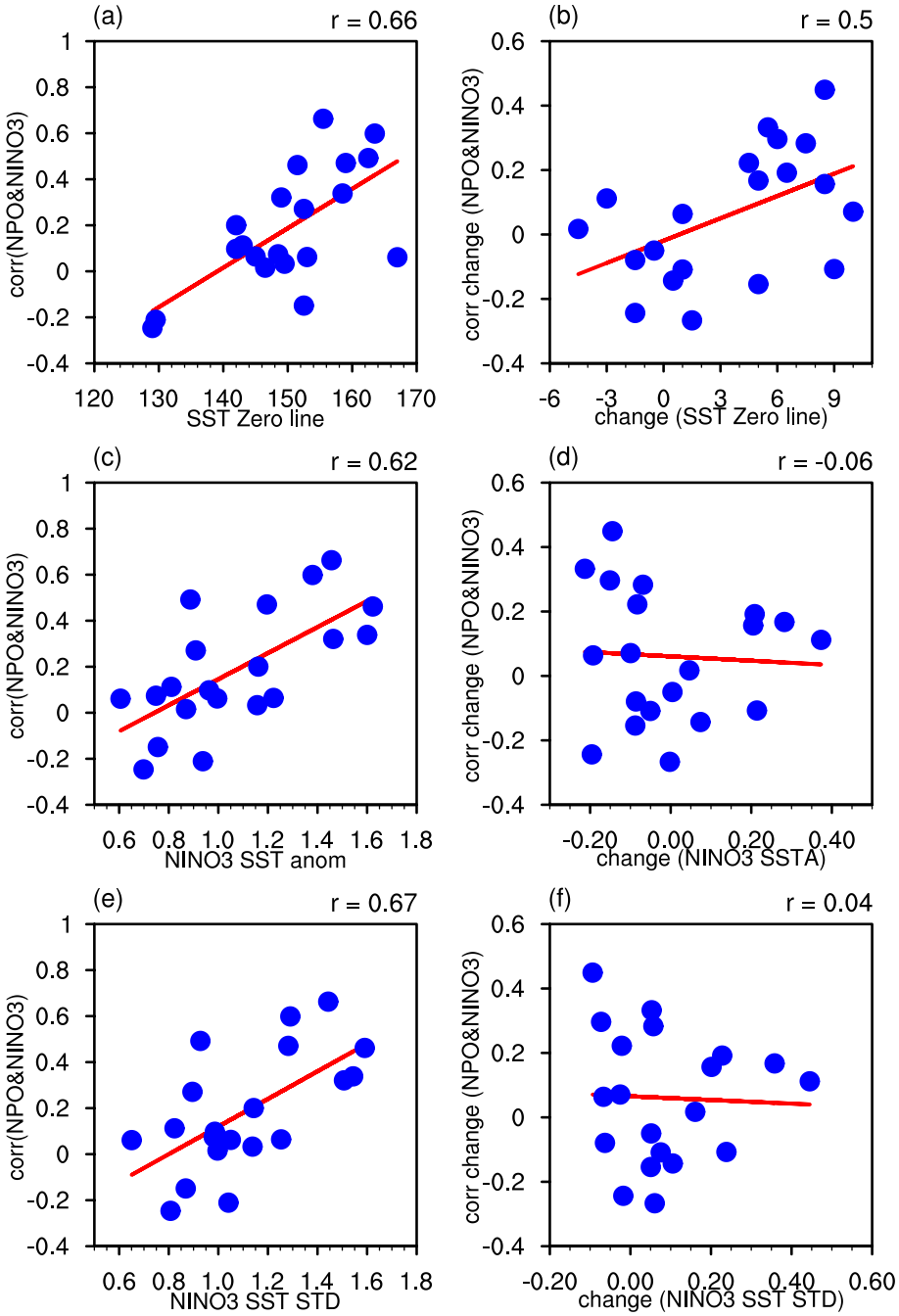

Fig. 14 Scatter plots between winter NPO–Niño3 correlations against **a** longitudinal locations of the 0 °C isoline of winter SST anomalies over the equatorial western Pacific, **c** winter SST anomalies averaged in the Niño3 region regressed upon the winter Niño3 index, and **e** standard deviations of the winter Niño3 index during 2033/34–2098/99 among the 20 models. Scatter plots between projected changes in the winter NPO–Niño3 correlation against projected changes in **b** longitudinal locations of the 0 °C isoline of winter SST anomalies over the equatorial western Pacific, **d** winter SST anomalies averaged in Niño3 region regressed upon the winter Niño3 index, and **f** standard deviations of the winter Niño3 index among the 20 models

the Group N models project a decrease in the winter ENSO-related SST anomalies in most parts the tropical Pacific (Fig. 16c). The ENSO-related precipitation anomalies are projected to be weakened over the tropical northern Pacific, together with an increase over the tropical southern Pacific (Fig. 16d). The projected decreases of SST in the tropical Pacific and precipitation in the tropical northern Pacific may weaken the ENSO-induced atmospheric teleconnection, leading to a decrease in the winter ENSO–AL relation. Hence, the uncertainty in the projected changes of the winter AL–ENSO relation across the models is partly related to various ENSO-related SST and precipitation changes over the tropical Pacific (Fig. 16e, f).

5 Summary and discussion

This study evaluates the simulations of the first two dominant modes of the North Pacific atmospheric variability in boreal winter, the AL and NPO patterns, as well as their relations to the North Pacific SLP, Eurasian and North American SAT and Pacific SST, by 20 coupled climate

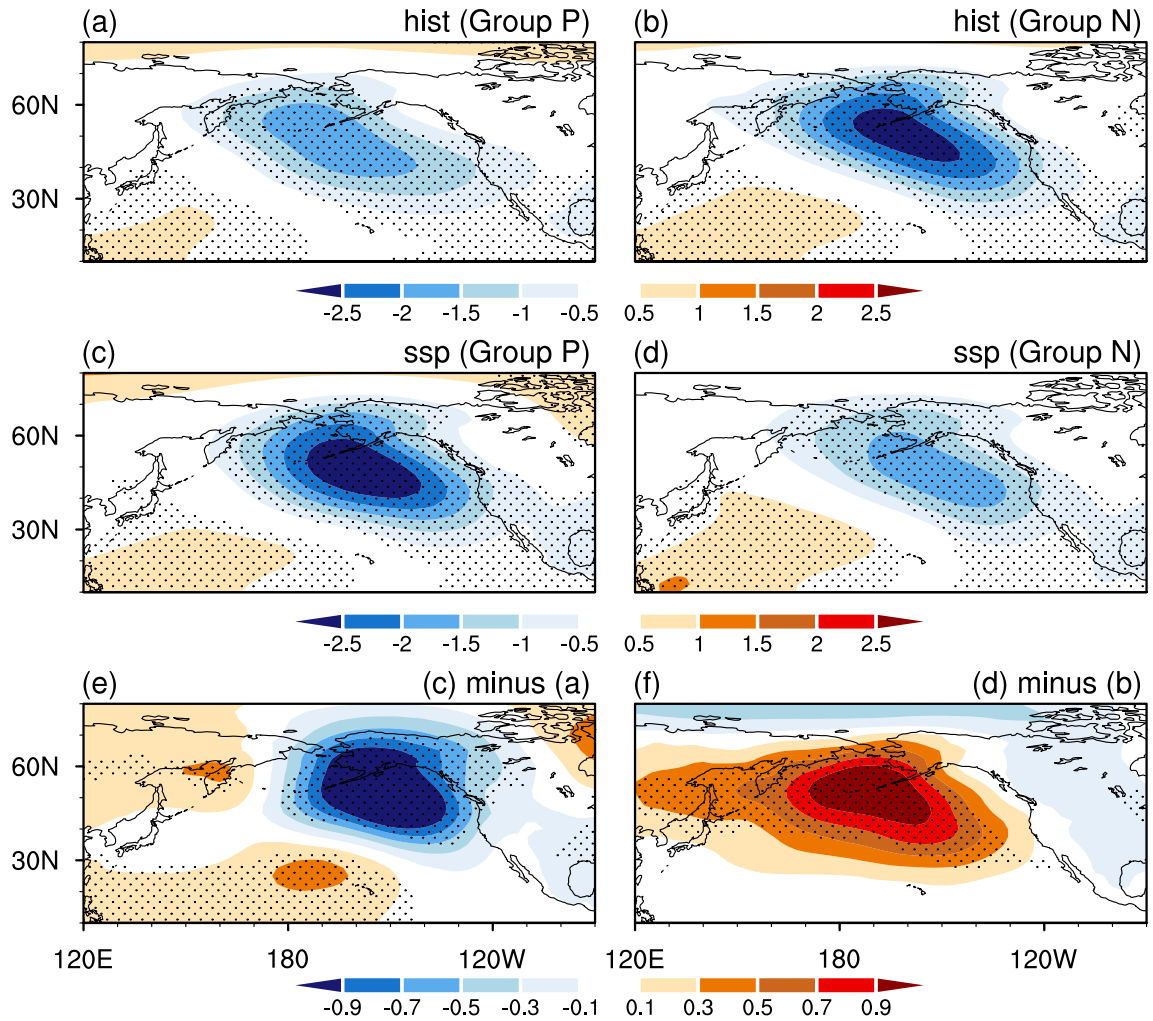

Fig. 15 Ensemble means of winter SLP anomalies (unit: hPa) regressed upon the winter Niño3 index over **a**, **b** 1948/49–2013/14 and **c**, **d** 2033/34–2098/99 for the **a**, **c** Group P and **b**, **d** Group N models. **e** Differences in the winter SLP anomalies regressed upon the winter Niño3 index between 2033/34–2098/99 and 1948/49–2013/14 for the Group P models. **f** As in **e**, but for the Group N models. Stippling regions in **a**–**d** indicate SLP anomalies significant at the 95% confidence level. Stippling regions in **e**, **f** indicate SLP differences that are significantly different from zero at the 95% confidence level. The models are selected as Group P (N) models when projected changes of the AL–ENSO correlation coefficient are higher than 0.1 (lower than − 0.1)

models for the IPCC AR6. The climate change projections of these behaviors, under the SSP2-RCP4.5 scenario, have also been analyzed.

In the historical simulations (1948/49–2013/14), all the models can reasonably well capture the winter AL, NPO, PDO and VM patterns, with spatial correlation coefficients between the observed and simulated patterns over 0.6. In addition, the ensemble mean of the 20 models can well simulate the winter AL and NPO related SAT anomalies over Eurasia and North America. The close relationships of the winter AL with PDO and ENSO, as well as the linkage of the winter NPO with the VM, could also be simulated by all the models. However, the observed connection of ENSO with the winter NPO cannot be captured by most models and the MME. There exists a large spread in the winter ENSO–NPO connection across the 20 models, which is likely attributed to the divergence of the zonal location of the ENSO-associated SST and precipitation anomalies over the tropical Pacific. In particular, a westward shift of the ENSO-related SST anomaly pattern would lead to westward movements of the tropical atmospheric convection and the induced atmospheric teleconnection over the North Pacific. As such, the winter ENSO-induced atmospheric anomalies project weakly on the NPO-related atmospheric anomalies, leading to a weak ENSO–NPO relationship. It is indicated that changes in the ENSO intensity also influence the winter NPO–ENSO relation. A model with a strong amplitude of ENSO tends to have a close winter NPO–ENSO relation. Yeh et al. (2018) reported that the southern center of the winter NPO-related SLP anomalies is located more eastward

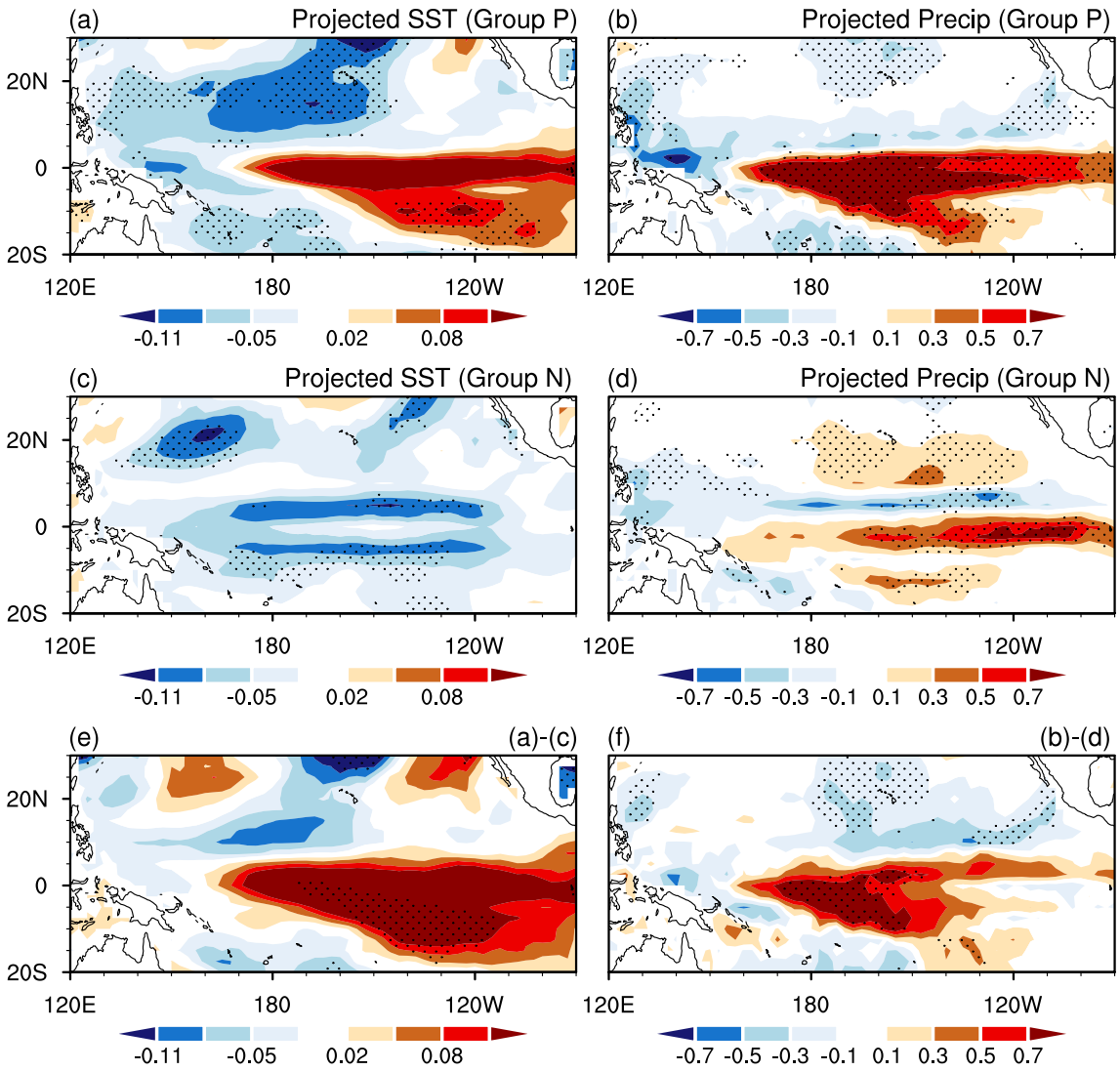

Fig. 16 Differences in the ensemble means of winter **a** SST (unit: °C) and **b** precipitation (unit: mm day^{-1}) anomalies regressed upon the winter Niño3 index for the Group P models between 2033/34–2098/99 and 1948/49–2013/14. **b**, **d** As in **a**, **b**, but for the Group N models. **e** Is the difference between **a** and **c**, **f** is the difference between **b** and **d**. Stippling regions in **a**–**f** indicate the differences that are significantly differently from zero at the 95% confidence level. The models are selected as Group P (N) models when projected changes of the AL–ENSO correlation coefficient are higher than 0.1 (lower than − 0.1)

after than before the mid-1990s based on observation and reanalysis data. They indicate that the eastward shift of the southern center of the NPO leads to a weakening of the simultaneous winter NPO–ENSO relation after the mid-1990s. Above evidence implies that differences in the spatial structure of the winter NPO may also have a contribution to the large spread of the winter NPO–ENSO relation among the CMIP6 models.

Under the SSP2-RCP4.5 scenario over the period of 2033/34–2098/99, centers of the winter AL tend to shift northward. However, the zonal movement of the center of the AL as well as the centers of the NPO show large uncertainties among the models. In addition, the projected changes in the amplitudes of the AL and NPO patterns also show high uncertainties across the 20 models. The projected changes in the amplitude of the AL have a close relation with the changes in the winter ENSO-related SLP anomalies over the mid-latitude North Pacific. This suggests that an increase (a decrease) in the strength of the ENSO-induced atmospheric teleconnection over the North Pacific may partly contribute to the projected increase (decrease) of the AL amplitude. Factors responsible for the uncertainty in projected changes of the NPO amplitude remain to be explored. Previous studies indicated that, besides the tropical ENSO forced influence, the interaction between the low-frequency mean flow and synoptic-scale eddies over the North Pacific

Table 2 The 15 models used in Fig. 17 that both participated in CMIP5 and CMIP6

Mode ID	CMIP5	CMIP6	Modeling centers
1	ACCESS1-0	ACCESS-CM2	CSIRO-ARCCSS, Australia
2	ACCES1-3	ACCESS-ESM1-5	CSIRO, Australia
3	BCC-CSM1-1-m	BCC-CSM2-MR	Beijing Climate Center, China
4	CanESM2	CanESM5	CCCma, Canada
5	CESM1-WACCM	CESM2-WACCM	NCAR, USA
6	CNRM-CM5	CNRM-CM6-1	CNRM-CERFACS, France
7	FGOALS-g2	FGOALS-g3	IAP-CAS, China
8	GFDL-ESM2G	GFDL-ESM4	NOAA-GFDL, USA
9	HadGEM2-AO	HadGEM3-GC31-LL	Met Office Hadley Centre, UK
10	IPSL-CM5A-LR	IPSL-CM6A-LR	IPSL, France
11	MIROC5	MIROC6	JAMSTEC, AORI, NIES, and and R-CCS, Japan
12	MIROC-ESM	MIROC-ES2L	JAMSTEC, AORI, and R-CCS, Japan
13	MPI-ESM-MR	MPI-ESM1-2-HR	Max Planck Institute for Meteorology, Germany
14	MRI-ESM1	MRI-ESM2-0	Meteorological Research Institute, Japan
15	NorESM1-M	NorESM2-LM	CICERO, NERSC, NILU, UiB, UiO, and UNI, Norway

also plays an important role in maintaining the AL and NPO. In addition, studies suggested that climate changes would adjust storm track activities (Bengtsson et al. 2006; Teng et al. 2008; Ulbrich et al. 2008), which also influence the strength of the atmospheric teleconnection and associated strengths of the AL and NPO. To what extent these high-frequency activities would respond to global climate change and further influence the AL and NPO patterns remain to be investigated.

The connections between the winter AL and PDO, AL and ENSO, and NPO and ENSO/VM are still robust over the forced period 2033/34–2098/99. Compared to those in the historical simulations, most models project a decrease of the NPO–VM relationship, indicating the winter NPO has a weak connection with the VM with global warming. However, there exists a large uncertainty in the projected changes of the winter AL–ENSO relation, which is partly due to various ENSO-related SST and precipitation changes over the tropical Pacific across the models. In particular, increases in the projected ENSO-related SST anomalies in the tropical Pacific would enhance precipitation and atmospheric convection over the tropical Pacific, which trigger an enhanced PNA-like atmospheric teleconnection over the North Pacific that contributes to the strengthening of the AL intensity, and result in a close winter ENSO–AL connection in a warming climate. The conditions are opposite for the models project decreases of the tropical SST anomalies.

In this study, we mainly focus on examining performances of the 20 CMIP6 models in simulating the winter AL and NPO and their relations with the dominant modes of the Pacific SST variability. One may ask whether there exists a model improvement in capturing spatial patterns of the winter AL, NPO, PDO and VM in the CMIP6 models compared to their previous versions participated in the CMIP5. Table 2 lists the 15 models that participated in both CMIP5 and CMIP6. Figure 17 compares the skill scores of the spatial patterns of winter AL, NPO, PDO, and VM in the historical simulations of these CMIP5 and CMIP6 models. The skill scores of the winter AL and NPO patterns are higher than those of the winter PDO and VM in both CMIP5 and CMIP6 (Fig. 17). In addition, for the ensemble mean, skill scores of the AL, PDO and VM patterns, especially the PDO, are higher in the CMIP6 than CMIP5 models (Fig. 17a, c, d). This indicates that the latest models have improvements in capturing the wintertime dominant AL, PDO and VM patterns, although the AL skill is already well in CMIP5. Skill scores of the NPO pattern are high and comparable for the CMIP5 and CMIP6 models (Fig. 17b). For individual models, about 67% of the models (i.e. 10 of the 15) show skill improvements in simulating the spatial patterns of the winter AL, PDO and VM (Fig. 17a, c, d). By contrast, only half of the models show skill improvements in simulating the NPO pattern (Fig. 17b). We have not compared other aspects of skills between the CMIP6 and CMIP5 models, such as relations of the winter AL with ENSO/PDO and relations of the winter NPO with ENSO/VM, which are also interesting and await further investigations.

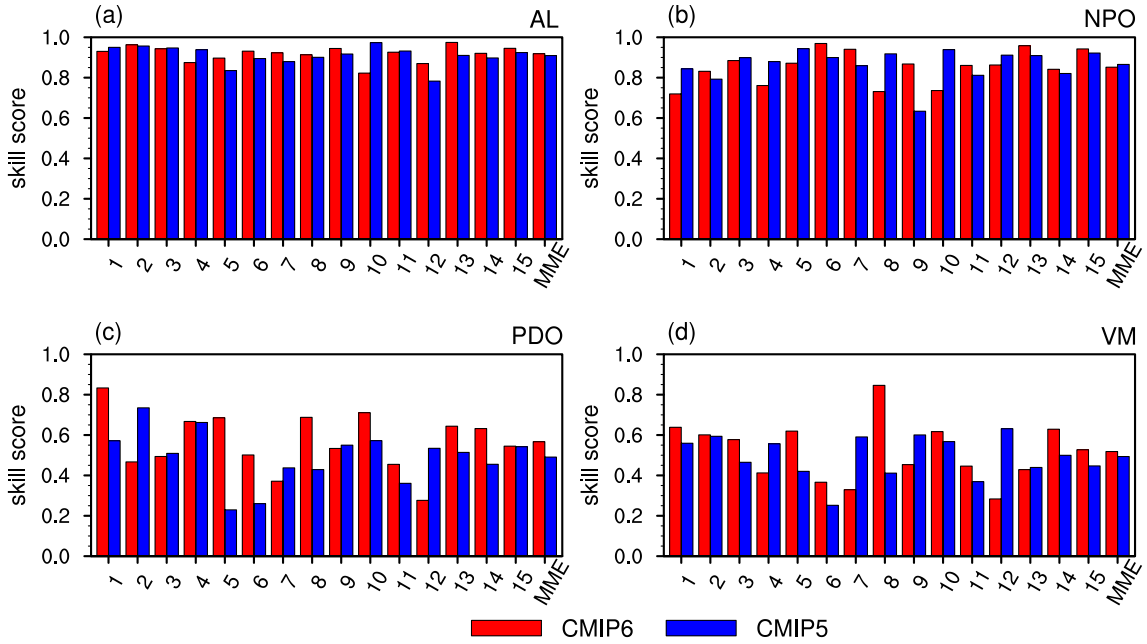

Fig. 17 Skill scores of the spatial patterns of winter **a** AL, **b** NPO, **c** PDO, and **d** VM for the historical simulations of 15 models participated in (blue bar) CMIP5 and (red bar) CMIP6. The MME result of the 15 models is also shown. Spatial pattern of the winter AL (NPO) is represented by winter SLP anomalies regressed upon the normalized winter AL (NPO) index over the North Pacific (15°–75° N and 120° E–120° W). Spatial pattern of the winter PDO (VM) is represented by winter SST anomalies regressed upon the normalized winter PDO (VM) index over 30° S–60° N, 120° E–120° W (10°–60° N, 120° E–120° W)

Acknowledgements We thank the three anonymous reviewers for their constructive suggestions, which helped to improve the paper. This study is jointly supported by the National Key Research and Development Program of China (Grant 2018YFA0605604), and the National Natural Science Foundation of China Grants (41605050, 41530425, and 41775080).

References

Alexander MA, Bladé I, Newman M, Lanzante JR, Lau NC, Scott JD (2002) The atmospheric bridge: the influence of ENSO teleconnections on air–sea interaction over the global oceans. J Clim 15:2205–2231

Barsugli JJ, Sardeshmukh PD (2002) Global atmospheric sensitivity to tropical SST anomalies throughout the Indo-Pacific basin. J Clim 15(23):3427–3442

Bengtsson L, Hodges KI, Roeckner E (2006) Storm tracks and climate change. J Clim 19:3518–3543

Bond NA, Overland JE, Spillane M, Stabeno P (2003) Recent shifts in the state of the North Pacific. Geophys Res Lett 30:2183. https://doi.org/10.1029/2003gl018597

Chen SF, Song LY (2018) Definition sensitivity: impact of winter North Pacific Oscillation on the surface air temperature over Eurasia and North America. Adv Atmos Sci 35:702–712

Chen W, Hans FG, Huang RH (2000) The interannual variability of East Asian winter monsoon and its relation to the summer monsoon. Adv Atmos Sci 17:48–60

Chen L, Yu YQ, Sun D (2013a) Cloud and water vapor feedbacks to the El Niño warming: are they still biased in CMIP5 models? J Clim 26:4947–4961

Chen W, Feng J, Wu RG (2013b) Roles of ENSO and PDO in the link of the East Asian winter monsoon to the following summer monsoon. J Clim 26:622–635

Chen L, Li T, Yu YQ (2015) Causes of strengthening and weakening of ENSO amplitude under global warming in four CMIP5 models. J Clim 28:3250–3274

Chen L, Li T, Yu YQ, Behera SK (2017) A possible explanation for the divergent projection of ENSO amplitude change under global warming. Clim Dyn 49:3799–3811

Chen Z, Gan B, Wu L, Jia F (2018) Pacific-North American teleconnection and North Pacific Oscillation: historical simulation and future projection in CMIP5 models. Clim Dyn 50:4379–4403

Chen SF, Chen W, Wu R, Yu B, Graf HF (2020) Potential impact of preceding Aleutian Low variation on the El Niño–Southern Oscillation during the following winter. J Clim 33:3061–3077

Cherchi A, Masina S, Navarra A (2012) Tropical Pacific-North Pacific teleconnection in a coupled GCM: remote and local effects. Int J Climatol 32(11):1640–1653

Chhak K, Di Lorenzo E, Schneider N, Cummins P (2009) Forcing of low-frequency ocean variability in the Northeast Pacific. J Clim 22:1255–1276

Choi J, Cha Y (2017) Anomalous variation in summer tropical cyclone activity by preceding winter Aleutian low oscillation. Atmos Sci Lett 18:268–275. https://doi.org/10.1002/asl.752

Davis RE (1976) Predictability of sea surface temperature and sea level pressure anomalies over the North Pacific ocean. J Phys Oceangr 6(3):249–266

Deser C, Phillips AS, Bourdette V, Teng H (2012) Uncertainty in climate change projections: the role of internal variability. Clim Dyn 38:527–546

Di Lorenzo E et al (2008) North Pacific Gyre Oscillation links ocean climate and ecosystem change. Geophys Res Lett 35:L08607

Di Lorenzo E et al (2010) Central Pacific El Niño and decadal climate change in the North Pacific. Nat Geosci 3:762–765
Ding RQ, Li JP, Tseng YH, Sun C, Guo Y (2015) The Victoria mode in the North Pacific linking extratropical sea level pressure variations to ENSO. J Geophys Res Atmos. https://doi.org/10.1002/2014jd022221
Eyring V, Bony S, Meehl GA, Senior CA, Stevens B, Stouffer RJ, Taylor KE (2016) Overview of the Coupled Model Intercomparison Project Phase 6 (CMIP6) experimental design and organization. Geosci Model Dev 9:1937–1958
Furtado JC, Di Lorenzo E, Schneider N, Bond NA (2011) North Pacific decadal variability and climate change in the IPCC AR4 models. J Clim 24:3049–3067
Furtado JC, Di Lorenzo E, Anderson BT, Schneider N (2012) Linkages between the North Pacific Oscillation and central tropical Pacific SSTs at low frequencies. Clim Dyn 39(12):2833–2846. https://doi.org/10.1007/s00382-011-1245-4
Gan B et al (2017) On the response of the aleutian low to greenhouse warming. J Clim 30:3907–3925
Ge Y, Gong G (2009) North American snow depth and climate teleconnection patterns. J Clim 22:217–233
Gershunov A, Barnett TP (1998) Interdecadal modulation of ENSO teleconnections. Bull Am Meteorol Soc 79:2715–2725. https://doi.org/10.1175/1520-0477(1998)079,2715:IMOET.2.0.CO;2
Harding KJ, Snyder PK (2015) The relationship between the Pacific-North American teleconnection pattern, the great plains low level jet, and North Central US heavy rainfall events. J Clim 28:6729–6742
Horel JD, Wallace JM (1981) Planetary-scale atmospheric phenomena associated with the Southern Oscillation. Mon Weather Rev 109:813–829
Hoskins BJ, Karoly DJ (1981) The steady linear response of a spherical atmosphere to thermal and orographic forcing. J Atmos Sci 38(6):1179–1196
Huang B et al (2017) Extended Reconstructed Sea Surface Temperature version 5 (ERSSTv5), Upgrades, validations, and intercomparisons. J Clim 30:8179–8205
Ji X, Neelin JD, Lee SK, Mechoso CR (2014) Interhemispheric teleconnections from tropical heat sources in intermediate and simple models. J Clim 27(2):684–697
Jo HS, Yeh SW, Lee SK (2015) Changes in the relationship in the SST variability between the tropical Pacific and the North Pacific across the 1998/1999 regime shift. Geophys Res Lett 42:7171–7178
Joshi MK, Ha KJ (2019) Fidelity of CMIP5-simulated teleconnection between Atlantic multidecadal oscillation and Indian summer monsoon rainfall. Clim Dyn 52:4157–4176
Kalnay E, Kanamitsu M, Kistler R, Collins W, Deaven D, Gandin L, Iredell M, Saha S, White G, Woollen J (1996) The NCEP/NCAR 40-year reanalysis project. Bull Am Meteorol Soc 77(3):437–471
Kim JW, Yeh SW, Chang EC (2014) Combined effect of El Niño–Southern Oscillation and Pacific decadal oscillation on the East Asian winter monsoon. Clim Dyn 42:957–971
Kucharski F, Joshi MK (2017) Influence of tropical south Atlantic sea surface temperatures on the Indian summer monsoon in CMIP5 models. Q J R Meteorol Soc 143:1351–1363
Latif M, Barnett TP (1996) Decadal climate variability over the North Pacific and North America: dynamics and predictability. J Clim 9:2407–2423
Lau NC (1988) Variability of the observed midlatitude storm tracks in relation to low-frequency changes in the circulation pattern. J Atmos Sci 45:2718–2743. https://doi.org/10.1175/1520-0469(1988)045,2718:VOTOMS.2.0.CO;2
Leung YT, Cheung HN, Zhou W (2017) Meridional displacement of the East Asian trough and its response to ENSO forcing. Clim Dyn 48:335–352
Linkin ME, Nigam S (2008) The north pacific oscillation-west Pacific teleconnection pattern: mature-phase structure and winter impacts. J Clim 21:1979–1997
Luo JJ, Behera SK, Masumoto Y, Yamagata T (2011) Impact of global ocean surface warming on seasonal-to-interannual climate prediction. J Clim 24:1626–1646
Mantua NJ, Zhang Y, Wallace JM, Francis R (1997) A Pacific interdecadal climate oscillation with impacts on salmon production. Bull Am Meteorol Soc 78:1069–1079
Matsuura K, Willmott CJ (2009) Terrestrial air temperature: 1900–2008 gridded monthly time series (version 5.01), University of Delaware Dept. of Geography Center. http://www.esrl.noaa.gov/psd/data/gridded/data.UDel_AirT_Precip.html. Accessed 23 July 2019
Namias J (1969) Seasonal interactions between the North Pacific Ocean and the atmosphere during the 1960's. Mon Weather Rev 97:173–192
Namias J (1972) Experiments in objectively predicting some atmospheric and oceanic variables for the winter of 1971–1972. J Appl Meteorol 11:1164–1174
Overland JE, Pease CH (1982) Cyclone climatology of the Bering Sea and its relation to sea ice extent. Mon Weather Rev 110:5–13
Pak G, Park YH, Vivier F, Kwon YO, Chang KI (2014) Regime-dependent nonstationary relationship between the East Asian Winter Monsoon and North Pacific Oscillation. J Clim 27(21):8185–8204
Park JY, Yeh SW, Kug JS, Yoon J (2013) Favorable connections between seasonal footprinting mechanism and El Niño. Clim Dyn 40:1169–1181
Pierce DW, Barnett TP, Schneider N, Saravanan R, Dommentget D, Latif M (2001) The role of ocean dynamics in producing decadal climate variability in the North Pacific. Clim Dyn 18:51–70
Rodionov SN, Overland JE, Bond NA (2005) The Aleutian low and winter climatic conditions of the Bering Sea. Part I: classification. J Clim 18:160–177
Rogers JC (1981) The North Pacific oscillation. J Climatol 1:39–57
Song LY, Duan WS (2015) Interannual relationship between the winter Aleutian low and rainfall in the following summer in South China. Atmos Ocean Sci Lett 8:271–276. https://doi.org/10.3878/AOSL20150021
Soulard N, Lin H, Yu B (2019) The changing relationship between ENSO and its extratropical response patterns. Sci Rep 9:6507. https://doi.org/10.1038/s41598-019-42922-3
Taylor KE (2001) Summarizing multiple aspects of model performance in a single diagram. J Geophys Res 106:7183–7192
Taylor KE, Stouffer RJ, Meehl GA (2012) An overview of CMIP5 and the experiment design. Bull Am Meteorol Soc 93(4):485–498
Teng H, Washington WM, Meehl GA (2008) Interannual variations and future change of wintertime extratropical cyclone activity over North America in CCSM3. Clim Dyn 30:673–686
Terada K, Hanzawa M (1984) Climate of the North Pacific Ocean. In: Van Loon H (ed) World survey of climatology, vol 15. Elsevier, Oxford, pp 431–504
Thompson DW, Wallace JM (1998) The Arctic Oscillation signature in the wintertime geopotential height and temperature fields. Geophys Res Lett 25(9):1297–1300
Thompson DW, Wallace JM (2000) Annular modes in the extratropical circulation. Part I: month-to-month variability. J Clim 13(5):1000–1016
Trenberth KE, Hurrell JW (1994) Decadal atmosphere-ocean variations in the Pacific. Clim Dyn 9:303–319

Trenberth KE, Branstator GW, Karoly D, Kumar A, Lau NC, Ropelewski C (1998) Progress during TOGA in understanding and modeling global teleconnections associated with tropical sea surface temperatures. J Geophys Res 103(C7):14291–14324. https://doi.org/10.1029/97jc01444

Ulbrich U, Pinto JG, Kupfer H, Leckebusch C, Spangehl T, Reyers M (2008) Changing northern hemisphere storm tracks in an ensemble of IPCC climate change simulations. J Clim 21:1669–1679

Vimont DJ, Battisti DS, Hirst AC (2001) Footprinting: a seasonal connection between the tropics and mid-latitudes. Geophys Res Lett 28:3923–3926. https://doi.org/10.1029/2001GL013435

Vimont DJ, Wallace JM, Battisti DS (2003) The seasonal footprinting mechanism in the Pacific: implications for ENSO. J Clim 16:2668–2675. https://doi.org/10.1175/1520-0442(2003)016,2668:TSFMIT.2.0.CO;2

Wallace JM, Gutzler DS (1981) Teleconnections in the geopotential height field during the northern hemisphere winter. Mon Weather Rev 109:784–812

Wang B, Wu R, Fu X (2000) Pacific-East Asian teleconnection: how does ENSO affect East Asian climate? J Clim 13:1517–1536

Wang X, Chen M, Wang C, Yeh S, Tan W (2019) Evaluation of performance of CMIP5 models in simulating the North Pacific Oscillation and El Niño Modoki. Clim Dyn 52:1383–1394

Wettstein JJ, Wallace JM (2010) Observed patterns of month-to month storm track variability and their relationship to the background flow. J Atmos Sci 67:1420–1437

Yeh SW, Kang YJ, Noh Y, Miller AJ (2011) The North Pacific climate transitions of the winters of 1976/77 and 1988/89. J Clim 24:1170–1183

Yeh SW, Wang X, Wang CZ, Dewitte B (2015) On the relationship between the North Pacific climate variability and the central Pacific El Niño. J Clim 28:663–677

Yeh SW, Yi DW, Sung MK, Kim YH (2018) An eastward shift of the North Pacific Oscillation after the mid-1990s and its relationship with ENSO. Geophys Res Lett 45:6654–6660

Yoon and Yeh (2010) Influence of the Pacific decadal oscillation on the relationship between El Niño and the northeast Asian summer monsoon. J Clim 23(17):4525–4537

Yu JY, Kim ST (2011) Relationships between extratropical sea level pressure variations and the central Pacific and eastern Pacific types of ENSO. J Clim 24:708–720

Yu B, Lin H (2019) Modification of the wintertime Pacific-North American pattern related North American climate anomalies by the Asian–Bering–North American teleconnection. Clim Dyn 53(1–2):313–328

Yu B, Shabbar A, Zwiers F (2007) The enhanced PNA-like climate response to Pacific interannual and decadal variability. J Clim 20:5285–5300

Zhou W, Wang X, Zhou TJ, Li CY, Chan JCL (2007) Interdecadal variability of the relationship between the East Asian winter monsoon and ENSO. Meteorol Atmos Phys 98:283–293

Zhu YL, Wang HJ (2010) The relationship between the Aleutian Low and the Australian summer monsoon at interannual time scales. Adv Atmos Sci 27:177–184. https://doi.org/10.1007/s00376-009-8144-1